ACS OMEGA

Open Access

http://pubs.acs.org/journal/acsodf

Article

Exploring Druggable Binding Sites on the Class A GPCRs Using the Residue Interaction Network and Site Identification by Ligand Competitive Saturation

Published as part of ACS Omega special issue "3D Structures in Medicinal Chemistry and Chemical Biology".

Tugce Inan,[‖] Merve Yuce,[‖] Alexander D. MacKerell, Jr.,[*] and Ozge Kurkcuoglu[*]

Cite This: *ACS Omega* 2024, 9, 40154−40171

Read Online

ACCESS | Metrics & More | Article Recommendations | Supporting Information

ABSTRACT: G protein-coupled receptors (GPCRs) play a central role in cellular signaling and are linked to many diseases. Accordingly, computational methods to explore potential allosteric sites for this class of proteins to facilitate the identification of potential modulators are needed. Importantly, the availability of rich structural data providing the locations of the orthosteric ligands and allosteric modulators targeting different GPCRs allows for the validation of approaches to identify new allosteric binding sites. Here, we validate the combination of two computational techniques, the residue interaction network (RIN) model and the site identification by ligand competitive saturation (SILCS) method, to predict putative allosteric binding sites of class A GPCRs. RIN analysis identifies hub residues that mediate allosteric signaling within a receptor and have a high capacity to alter receptor dynamics upon ligand binding. The known orthosteric (and allosteric) binding sites of 18 distinct class A GPCRs were successfully predicted by RIN through a dataset of 105 crystal structures (91 ligand-bound, 14 unbound) with up to 77.8% (76.9%) sensitivity, 92.5% (95.3%) specificity, 51.9% (50%) precision, and 86.2% (92.4%) accuracy based on the experimental and theoretical binding site data. Moreover, graph spectral analysis of the residue networks revealed that the proposed sites were located at the interfaces of highly interconnected residue clusters with a high ability to coordinate the functional dynamics. Then, we employed the SILCS-Hotspots method to assess the druggability of the novel sites predicted for 7 distinct class A GPCRs that are critical for a variety of diseases. While the known orthosteric and allosteric binding sites are successfully explored by our approach, numerous putative allosteric sites with the potential to bind drug-like molecules are proposed. The computational approach presented here promises to be a highly effective tool to predict putative allosteric sites of GPCRs to facilitate the design of effective modulators.

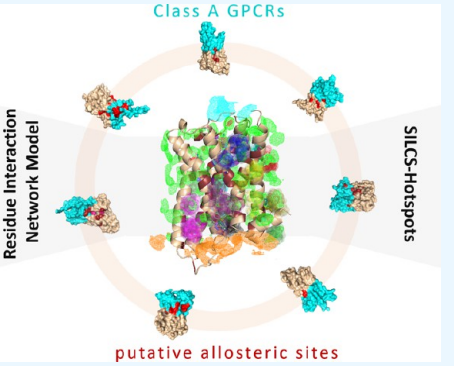

INTRODUCTION

G protein-coupled receptors (GPCRs) are 7-transmembrane receptors that govern numerous physiological effects triggered by external ligand binding to their extracellular orthosteric binding sites.[1] As they are implicated in many diseases and are easily accessible, many commercially successful medications within the pharmaceutical sector have been designed to selectively interact with GPCRs.[2] Approximately 17% of all approved drugs have been developed to bind GPCRs or similar protein structures.[2] Among these, class A GPCRs or rhodopsin-like receptors constitute the major therapeutic target for numerous medical conditions,[3] and over 500 drugs have been developed for class A GPCRs to date.[4] Of these, over 8% of the targets are chemokine, prostanoid, and melanocortin receptors.[4] Medical conditions treated targeting the class A GPCRs include diverse disease states such as allergic responses, cardiovascular diseases, hypertension, pulmonary diseases, depression, migraine, glaucoma, Parkinson's disease, schizophrenia, and alleviation of cancer-related fatigue.[2]

Besides their conserved orthosteric sites, GPCRs also include allosteric sites, where endogenous ligands such as ions, lipids, and peptides, and exogenous small molecules can bind and modulate the protein activity.[5,6] Allosteric modulators, unlike orthosteric ligands, are not competitive inhibitors; they act in either a positive or negative fashion, thereby increasing or decreasing the protein's activity.[7] Allosteric sites are typically less conserved than orthosteric sites, which display high topological and sequence conservation in the class A GPCRs. Therefore, allosteric sites offer the

Received: July 3, 2024
Revised: September 4, 2024
Accepted: September 6, 2024
Published: September 13, 2024

https://doi.org/10.1021/acsomega.4c06172
ACS Omega 2024, 9, 40154−40171

potential for better selectivity making them interesting target sites in proteins for novel, low-side-effect treatments.[5,8,9]

Numerous GPCR structures complexed with orthosteric and allosteric ligands are deposited in the GPCR database,[10] which enables the comparison of binding sites and ligands for all classes of GPCRs. The database also includes state-specific (active/inactive) structure models of GPCRs constructed using AlphaFold2-MultiState.[10,11]

Understanding the allosteric regulation in protein structures on a molecular level can facilitate structure-based allosteric drug design (SBADD). Protein topological analyses, including graph theory, statistical coupling analysis, and perturbation algorithms, have served as the starting point for many of the early computational attempts to understand allosteric communication.[12−15] Protein contact networks can understand coordinated structural motions by capturing energy transmissions along the shortest allosteric pathways.[16] Similarly, residue interaction network (RIN) models can reveal the wiring of the protein topology by pointing to residues with a high capacity to receive or send allosteric signals in the form of perturbations within the protein structure.[17,18] Anisotropic network model[19] and Gaussian Network Model[20] coupled with normal-mode analysis (NMA) are computationally efficient methods that make use of the conformational changes related to allostery.[21−25] Low-frequency motions that involve the mobility of multiple residues often explain the long-range nature of allosteric communication well; on the other hand, higher-frequency local motions are also taken into consideration to reveal the local effects in allosteric mechanisms.[26−28] Moreover, studying dynamic conformational ensembles is a commonly used and trusted approach to revealing allosteric mechanisms and allosteric residues.[29] Here, proteins are assumed to exist in a variety of conformations around their natural states, which can be distinguished by their energy landscape.

Beyond the identification of allosteric residues, SBADD requires the identification of ligand-binding pockets. All pockets and cavities,[30] as well as tunnels,[31] formed by protein topology, can be determined using different techniques; however, these cavities or tunnels may not necessarily accommodate drug-binding sites. Among binding site discovery methods, FTMap[32,33] has been highly popular using organic probes for fragment-based screening. While it is a rigid docking methodology, the dynamics of the protein may be considered by using molecular dynamics simulations[34] or elastic network models[35] to generate multiple protein conformations. While this facilitates the use of FTMap[32,33] to reveal cryptic sites that may be hidden in experimental structures, mixed solvent or cosolute simulations have been of great utility for identifying hidden pockets.[36−41] Among these, DruGUI uses isopropanol, isopropylamine, acetic acid, and acetamide as probes and estimates binding free energy to predict the hot spots on the protein surface.[37] Using this method, a pharmacophore model can be created by scoring the probes and identifying the high-affinity residues in the target protein.[42] The most extensive cosolute approach has been developed by MacKerell and co-workers by combining MD and oscillating chemical potential grand canonical Monte Carlo (GCMC)[43] simulations to develop the site identification by ligand competitive saturation (SILCS)[44] technology. This method uses a collection of aliphatic, aromatic, polar neutral, and charged solutes along with water molecules to map the functional group affinity pattern of the protein structure. Once the functional group affinity pattern has been converted into free energies, MC docking can be employed to identify and quantify the binding sites of a large number of chemical fragments, information that may be used to find druggable sites and advance pharmacophore design.[45−47]

In this study, we combined RIN and SILCS to detect ligand-binding orthosteric and allosteric sites on GPCRs with high accuracy and precision through validation against experimental 3D structures. Contact topology-focused RIN can pinpoint the subtype-specific critical residues of the GPCRs, as shown by a statistical analysis of a dataset of class A GPCRs involving 105 crystal structures. RIN also identified potential allosteric sites. Then, we conducted SILCS calculations to reveal the druggability of the predicted allosteric regions for seven GPCRs, namely the adenosine A1 receptor (A_1R), β2-adrenergic receptor (β_2AR), chemokine receptor CXCR2, dopamine receptor D1 (DRD1), free fatty acid receptor (FFA1, also known as GPR40), M2 muscarinic acetylcholine receptor (M2), and active/inactive conformers of the delta-opioid receptor (OPRD). The systematic approach presented in this study offers a highly effective method that incorporates contact topology information and fragment-based searching to detect allosteric druggable sites of GPCRs.

MATERIALS AND METHODS

Dataset and Protein Preparation. We investigated 18 different class A GPCRs. Supporting Information Table S1 lists these structures along with their protein data bank[48] (PDB) IDs, ligand names, ligand function (agonist, partial agonist, antagonist, and inverse agonist), and their binding sites as retrieved from GPCRdb.[49] The dataset contains 91 ligand-bound and 14 unbound GPCR structures. The majority of the ligand-bound structures contain multiple drugs that target distinct binding sites. The dataset thus samples numerous binding sites on the class A GPCRs, including orthosteric binding sites, intracellular, extracellular, and extrahelical allosteric sites, and a sodium ion binding site.[4]

Before implementing the residue interaction network (RIN) model, all ligands, ions, crystal water molecules, and any membrane components were removed from the structures. For the SILCS calculations, the missing loops of the crystal structures for A_1R, CXCR2, and DRD1 were completed utilizing Modeller 10.4,[50] where the models with the lowest DOPE scores were selected. Previous publications provide detailed instructions on the preparation of β_2AR,[45,51] FFA1 (also known as GPR40),[45] M2,[45] and OPRD[52] for the SILCS calculations.

Residue Interaction Network Model. The residue interaction network (RIN) model depicts the protein structure as a network of interconnected nodes, where nodes are placed at the α carbon atoms of residues linked to each other if they have atom−atom neighboring within a cutoff distance of 4.5 Å. This distance threshold incorporates van der Waals and electrostatic interactions. The length of the edges is calculated based on the local interaction force or affinity between residue pairs, a_{ij}[17,18]

$$a_{ij} = \frac{N_{ij}}{\sqrt{N_i N_j}} \quad (1)$$

Here, N_{ij} represents the total number of heavy atom pairs between the ith and jth nodes. Weighting N_{ij} by the total number of atoms (N_i and N_j) eliminates the effect of the amino

https://doi.org/10.1021/acsomega.4c06172
ACS Omega 2024, 9, 40154−40171

acid size. Node pairings with a high interaction strength are deemed to be more closely related. Thus, the length of edges between two adjacent nodes can be modeled as $1/a_{ij}$.[18] This formulation suppresses the bias toward covalently bonded interactions and accounts for both covalent and long-range interactions.

The centrality measure of betweenness identifies the frequently visited nodes or "hubs" of the network based on calculated shortest paths. The betweenness (C_B) value is calculated as follows[53]

$$C_B(l) = \sum_{i \neq j \neq l} \frac{s_{ij}(l)}{s_{(ij)}} \quad (2)$$

Here, s_{ij} is the number of shortest routes between nodes i and j, and $s_{ij}(l)$ is the number of shortest routes between nodes i and j that pass through node l. In this regard, nodes with high C_B values in the residue network have a high probability of residing on allosteric communication pathways that can be evaluated as novel drug targets.[18,54,55]

Similar to a previous study,[56] the spectral analysis of the network is carried out to cluster nodes for determining residue neighborhoods or domains, by studying the eigenspace of the N × N Laplacian matrix L satisfying the following expression,

$$U^T L U = \sum_{i,j} w_{ij}(u(i) - u(j))^2 \quad (3)$$

Here, the summation is pairwise for all ith and jth nodes linked with a weighted edge w_{ij} for a vector U in the eigenspace. The lowest nonzero eigenvalue corresponds to the Fiedler vector giving the largest node cluster for the residue network. Grouping the values as negative and positive, whose values change between $[-1, 1]$, reveals the nodes forming distinct clusters. Progressing from the low to high eigenvalues in the eigenspace, the sizes of the clusters diminish leading to the isolated edges in the limit. In this study, the three lowest nonzero eigenvectors are used to divide the protein structure into node clusters.

Binding Site Prediction Protocol with SILCS. The SILCS software suite (SilcsBio, LLC) was used to independently conduct SILCS oscillating μ_{ex} Grand Canonical Monte Carlo (GCMC)/MD simulations under the following procedure.[43,57,58] All of the systems included a membrane composed of 90/10 POPC and cholesterol that were constructed using CHARMM36m force field parameters[59] in conjunction with CHARMM-GUI.[60] Each system was subjected to 10 individual simulations yielding a total of 1 μs of MD simulation sampling (100 ns × 10). From the membrane-bound GPCRs 10 starting conformers were generated for the SILCS simulations by rotating the χ1 dihedral of side chains exposed to solvent in increments of 36° if their solvent accessibility was larger than 0.5 Å^2. GROMACS[61] was used to introduce solutes including benzene, propane, methanol, formamide, dimethyl ether, imidazole, acetate, and methylammonium to obtain a concentration of ∼0.25 M along with water at ∼55 M into the systems.[62] Solute parametrization was done using CHARMM General Force Field (CGenFF)[63] and the TIP3P model was used for water.[64] The solutes and water molecules near the GPCRs were subjected to equilibration using 25 cycles of GCMC. Then, the systems were further equilibrated using 100 cycles of 200,000 GCMC steps for both the water and solute molecules, a 5000-step steepest descent minimization, and a 100 ps MD equilibration. This was followed by a 1 ns long production MD simulation. Water molecules and solute molecules were exchanged between their gas phase and the protein structure during the GCMC steps. MD simulations were started from the final step of GCMC configuration. A harmonic force with a constant of 0.12 kcal/mol/Å^2 was applied to the C_α atoms during the MD simulations to avoid extreme conformational rearrangements.

To calculate the SILCS FragMaps, conformers collected every 10 ps from the MD simulations were used to calculate probability distributions of chosen solute atoms in 1 Å^3 grid elements. The probability distributions were normalized using a solute concentration based on one solute molecule for every 55 water molecules. The FragMaps probabilities were converted to grid free energies (GFE) by applying the Boltzmann transformation to the normalized probability distributions. FragMaps were used in conjunction with "generic" maps that pertain to the following physicochemical features; apolar (benzene and propane Cs), hydrogen bond donors (formamide N and imidazole protonated N), hydrogen bond acceptor (O atoms of formamide and dimethyl ether, and unprotonated N atom of imidazole), alcohol (methanol O), positive donor (methylammonium N), and negative acceptor (acetate carbonyl C).

SILCS-Hotspots was utilized to identify fragment-binding sites following the published protocol.[58] Briefly, the simulation systems were partitioned into 10 × 10 × 10 Å^3 subvolumes in which MC sampling of the fragment was performed. Fragments included mono- and bicyclic compound fragments, referred to as ring fragments, that were MC docked into every subvolume. The Metropolis criteria for the MC docking was based on Ligand Grid Free Energy (LGFE) scores and CGenFF intramolecular energy. LGFEs were calculated as the sum of the GFE values assigned to classified atoms in each ligand associated with the FragMap type to which that atom corresponds. Each fragment was subjected to 1000 MC docking runs in each 1000 Å^3 subvolume. Final fragment selection and Hotspot identification were performed using multiple rounds of spatial clustering using a 3 Å cluster radius according to the fragment's centers of mass. The Hotspots were ranked based on the mean LGFE scores over all the fragments located in each site.

Statistical Analysis. We calculated the sensitivity (SN), specificity (SP), precision (PRE), and accuracy (ACC) of the orthosteric and allosteric drug-binding site prediction for the class A GPCRs as follows,

$$SN = \frac{TP}{TP + FN} \quad (4)$$

$$SP = \frac{TN}{FP + TN} \quad (5)$$

$$PRE = \frac{TP}{TP + FP} \quad (6)$$

$$ACC = \frac{TP + TN}{TP + FP + TN + FN} \quad (7)$$

The quantities of true positives (TPs), true negatives (TNs), false positives (FPs), and false negatives (FNs) were obtained using four different drug-binding-site data sets. (i) Experimental ligand-binding sites: extracted from biochemical and crystallographic data provided for each ligand using the

https://doi.org/10.1021/acsomega.4c06172
ACS Omega 2024, 9, 40154−40171

PDBsum server;[65] (ii) theoretical ligand-binding sites: formed by the residues neighboring the ligand within a cutoff distance of 6.0 Å in the crystal structure; (iii) second shell residues of experimental binding sites; and (iv) second shell residues of theoretical binding sites, as computed in our previous study.[27] Second shell residues are the closest neighbors to experimental and theoretical binding sites based on α carbon atom distances of 5.0 Å or less. Additionally, the Z-score of the predicted residue i, Z_i, was calculated as follows:

$$Z_i = \frac{r_i - \bar{r}_i}{\sigma} \tag{8}$$

The closest distance between the predicted residue i and the experimental binding site is denoted by r_i. $\bar{r}_i$ is the mean distance for all predicted residues, and $\boldsymbol{\sigma}$ is the standard deviation. Z_i is negative when r_i is below the mean distance $\bar{r}_i$, and a higher negative Z-score indicates the proximity of the predicted residue to the experimental binding site. A mean Z-score was computed for all hub residues.

RESULTS AND DISCUSSION

Statistical Analysis for Binding Site Prediction of the Residue Interaction Network Model. To evaluate the success of the residue interaction network model (RIN) in predicting known ligand-binding sites, statistical analysis was performed on a total of 105 crystal structures (91 ligand-bound and 14 ligand-free) of 18 distinct class A GPCRs. It is important to mention that RIN calculations were carried out for the crystal structures without the ligands, i.e. the location of the orthosteric and allosteric ligands were unknown to the network model in the determination of the hub residues. The residues with high betweenness values, called hub residues, are assumed to have the ability to transmit a perturbation through residue−residue contacts. These residues were shown to have a high capacity to take a role in allosteric communication, thus they plausibly mark a ligand-binding site.[18,66] For the statistical analysis, four reference data sets were used to assess the binding site prediction ability of RIN through hub residues:

(i) the experimental dataset with known ligand-binding residues
(ii) the experimental dataset with known ligand-binding residues and their closest neighbors (the second shell within a cutoff of 5.0 Å distance between α carbon atoms)
(iii) the theoretical dataset containing the residues within a cutoff of 6.0 Å to the ligand
(iv) the theoretical dataset with the ligand-binding residues and their closest neighbors.

The statistics based on the hub residues predicted for 18 distinct class A GPCRs are presented in Supporting Information Table S1. As multiple holo-structures were investigated for each GPCR, rich binding site information was gathered from multiple ligands bound to the orthosteric and allosteric sites. The experimental binding site residues interacting with a ligand in a specific site were collected and included in the statistical analysis as a group. For example, the agonists ADO and PSB36 and antagonist DU172 bind to the orthosteric site of A_1R (Supporting Information Figure S1a). The residues interacting with these ligands were collected from the PDBsum server and referred to as the experimental orthosteric binding site residues in the statistical analysis. The statistical analysis was carried out for the second shell residues to consider the low resolution of the structural data. The theoretical dataset and the second shell residues were also investigated to understand if the method can predict the binding site regions of proteins with a low number of crystal structures. RIN predicted 4 true positives (Y12, T91, W247, and H251) on the orthosteric binding site of A_1R (Table S1 and Figure S1a) with 16.7% sensitivity, 87.1% specificity, 10% precision, and 81.5% accuracy. Here, the low sensitivity and precision are due to the other hub residues determined for the protein structure that may be either evaluated as allosteric sites or residues critical in allosteric communication. When the second shell residues were included in the calculations, the number of true positives increased to 12 for A_1R, improving all statistics. Considering the theoretical dataset and its second shell further improved the number of true positives for the orthosteric binding region of A_1R, achieving 48.7% sensitivity, 90.4% specificity, 47.5% precision, and 84.1% accuracy. The true positives on four reference data sets predicted by RIN on the orthosteric region of A_1R are marked as red spheres in Figure S1a. Overall, the orthosteric binding sites were successfully predicted by RIN for 18 distinct class A GPCR with up to 77.8% sensitivity, 51.9% precision, 92.5% specificity, and 86.2% accuracy, based on all four data sets. Here, the statistics were noted to remarkably increase either with the inclusion of more crystal structures in the experimental dataset or by extending the dataset to the theoretical second shell.

The same approach was followed for the statistical analysis of predicting known allosteric sites. The richness of the structural data highlights numerous allosteric binding sites with various ligands on GPCR class A proteins. For example, the β2-adrenergic receptor (β_2AR) has three distinct allosteric sites that accommodate the NAM AS408 and Cmpd-15P bound to the allosteric site 1 (extrahelical allosteric site) and allosteric site 3 (intracellular allosteric binding site), while the positive allosteric modulator (PAM) Cmpd-6FA bound to the allosteric site 2.[67] RIN also accurately predicted the known allosteric drug binding regions on GPCR class A proteins. For instance, when the experimental dataset of β_2AR was considered, the sensitivity and precision values were 11.1 and 1.8%, respectively, if at least 1 true positive was predicted for a distinct allosteric site. When the second shell residues were included, the number of true positives as well as sensitivity and precision percentages improved. On the other hand, RIN predicted no true positives on experimental and theoretical binding sites for the CC chemokine receptor 7 (CCR7) in complex with the allosteric antagonist Cmp2105,[68] where the calculations were done for one crystal structure. However, it predicted 1 true positive (Y96) on the experimental second shell and 2 true positives (Y96, N99) on the theoretical second shell dataset on the intracellular allosteric binding pocket. Similarly, the allosteric binding site residues (agonist INT-777 bound region)[69] on GPBAR and allosteric binding site 2 (BPTU bound region, lipidic interface)[70] on the P2Y1 receptor were predicted when the second shell residues were included. Since RIN is based on the contact topology of the protein, it is important to include numerous structures in the analysis. Nonetheless, the model can correctly predict the location of the allosteric binding sites based even on one crystal structure.

The statistical analysis confirmed that the hub residues indeed mark the orthosteric and known allosteric sites for the whole dataset of 105 GPCR class A structures. To further evaluate the significance of the predictions, a Z-score analysis was performed considering the hub residues and the

https://doi.org/10.1021/acsomega.4c06172
ACS Omega 2024, 9, 40154−40171

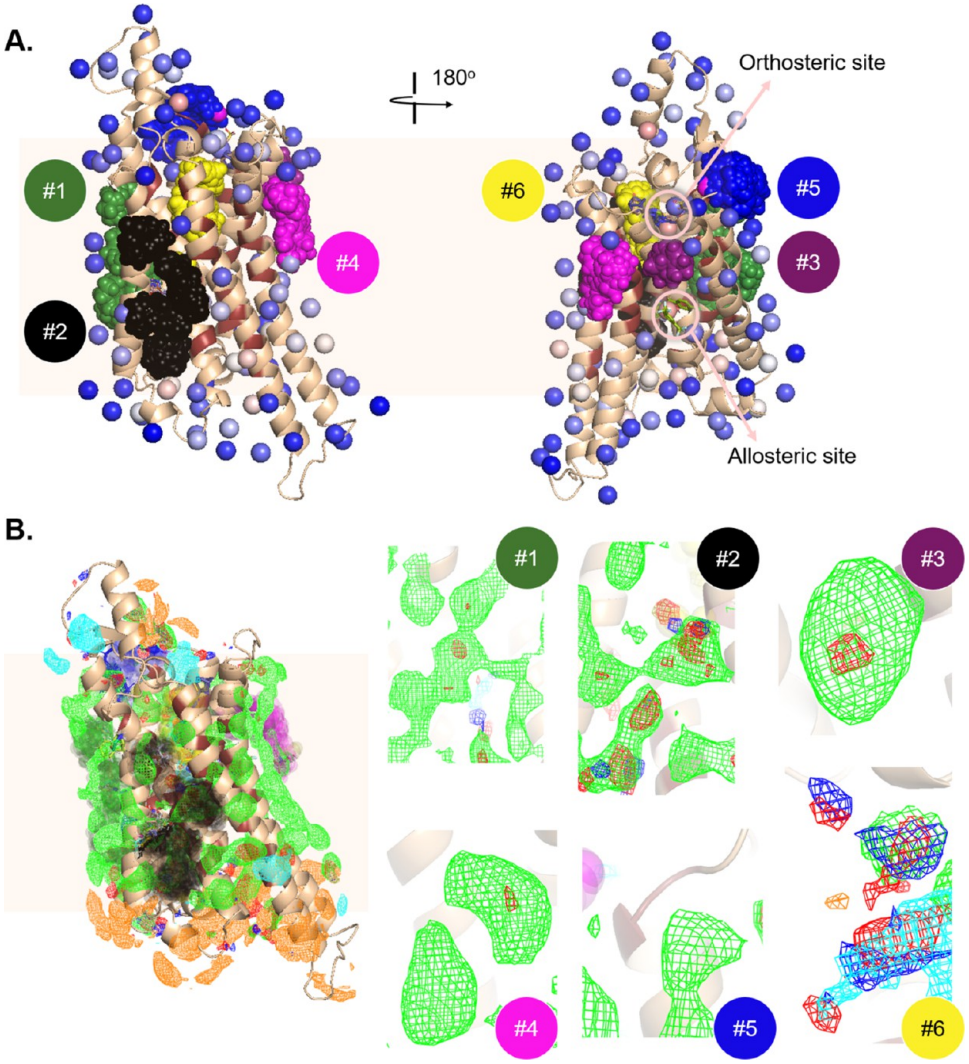

Figure 1. RIN and SILCS calculations predicted the known binding sites and proposed six putative allosteric sites for A_1R. (A) Structure of A_1R (tan cartoon) with the SILCS-Hotspots (vdW spheres, colored by ranking from least favorable mean LGFE (blue) to most favorable mean LGFE (red)) from two perspectives. Hub residues in the residue interaction network are colored in ruby in the cartoon representation. Fragments on Hotspots associated with proposed sites (#1−6) are displayed as spheres. The details of the site prediction are given in Table S2. (B) FragMaps displayed on the structure for each site in mesh including the apolar (green, − 0.9 kcal/mol), H-bond donor (blue, − 0.9 kcal/mol), H-bond acceptor (red, − 0.9 kcal/mol), negative (orange, − 1.2 kcal/mol), and positive (cyan, − 1.2 kcal/mol) FragMap types.

experimental drug-binding site dataset for the orthosteric and allosteric sites of the investigated receptors. A Z-score < − 1.0 indicates that the residue is close to the ligand-binding site, suggesting a function in binding and/or a role in the allosteric mechanism of the protein. Z-scores of the hub residues are given in Supporting Information Figures S1−S18 separately for the orthosteric and allosteric sites. True positives predicted on the orthosteric, and allosteric experimental binding sites are marked in red. Mean Z-scores for the orthosteric, and allosteric sites were at least −1.93 (CCR2) and −1.36 (B_2AR), respectively. With a more focused look, the majority of the mean *Z*-scores were around −2.0 highlighting the success of the RIN model in predicting known allosteric residues based on structures without the inclusion of ligands in the calculations.

Determination of the Putative Allosteric Binding Sites. Among the dataset, SILCS GCMC-MD simulations of 7 class A GPCR structures, namely adenosine A1 receptor (A_1R), β2-adrenergic receptor (β_2AR), chemokine receptor CXCR2, dopamine receptor D1 (DRD1), free fatty acid receptor (FFA1, also known as GPR40), muscarinic receptor type 2 (M2), and δ-opioid receptor (OPRD) were performed. SILCS simulations and subsequent SILCS-Hotspots[45] were used to assess the druggability of putative allosteric sites for the class A GPCRs that were suggested by the RIN model. The SILCS method provides a detailed map of potential fragment binding sites on the target protein. This method incorporates extensive fragment screening in the field of the FragMaps with SILCS-MC docking and fragment clustering. Consequently, it identifies potential fragment binding sites, or Hotspots, and prioritizes them based on mean LGFE scores or other user-selected metrics.

For the identification of binding sites appropriate for drug-like molecules, first, Hotspots next to the hub residues within a distance of 5 Å were considered. Not only the most favorable Hotspots based on mean LGFE scores but also sites with adjacent Hotspots were preferred based on the assumption that 2 or more fragments need to be linked to create drug-like

https://doi.org/10.1021/acsomega.4c06172
ACS Omega 2024, 9, 40154−40171

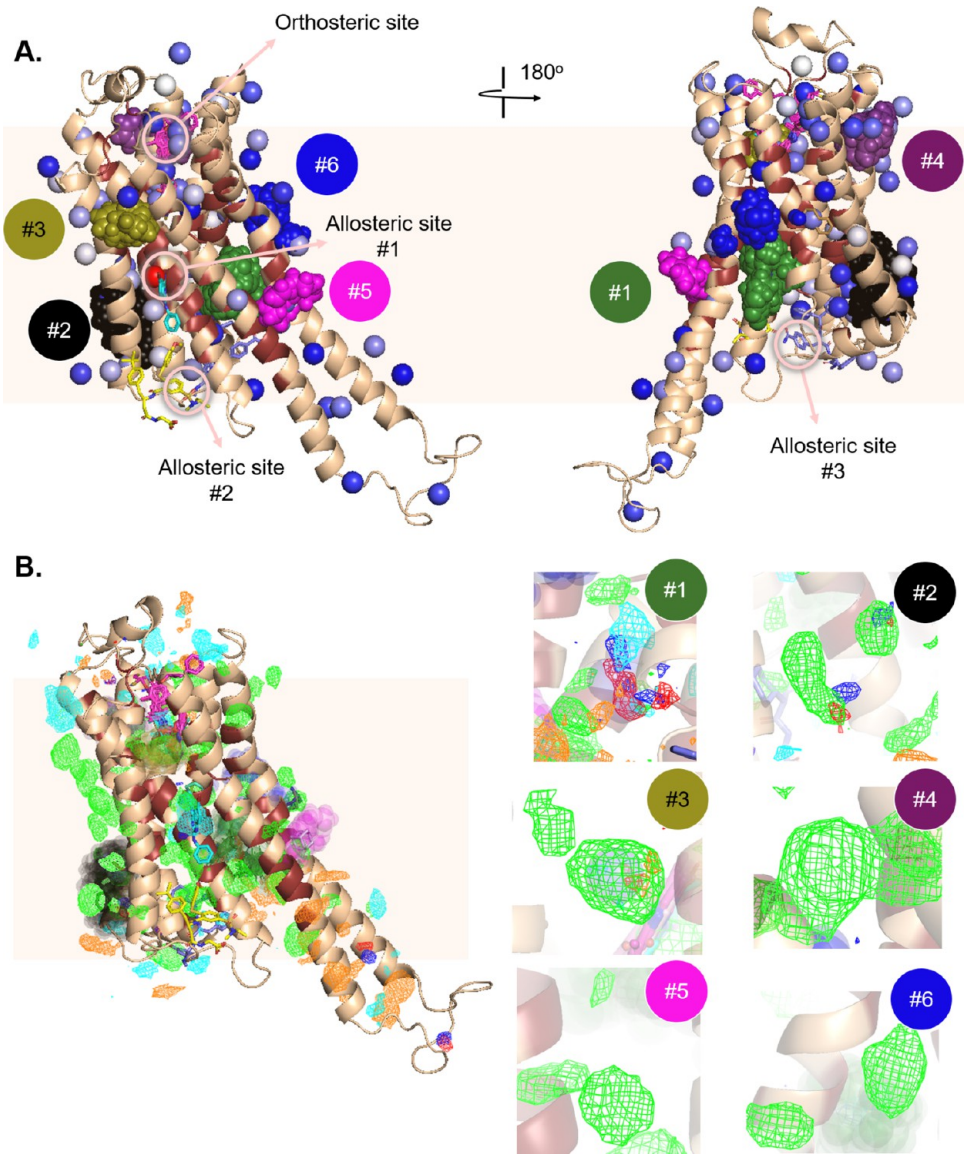

Figure 2. RIN and SILCS findings for β_2AR. (A) Structure of β_2AR (tan cartoon) with the SILCS Hotspots (vdW spheres colored from least favorable mean LGFE (blue) to red (most favorable mean LGFE)) and the hub residues (in ruby) is shown from two perspectives. Fragments on Hotspots associated with proposed sites (#1−6) are displayed as spheres. Details of the site prediction are given in Table S3. (B) FragMaps displayed on the structure for each site in mesh, explicitly showing the generic apolar (green, −0.9 kcal/mol), generic H-bond donor (blue, −0.9 kcal/mol), generic H-bond acceptor (red, −0.9 kcal/mol), negative (orange, −1.2 kcal/mol), and positive (cyan, −1.2 kcal/mol) FragMap types.

molecules (molecules with molecular weight >200 Da). Furthermore, the number of fragments in the Hotspots of interest was considered for binding site prediction. In the following, we first discussed the findings for the known binding sites, i.e., orthosteric and allosteric, if the investigated crystal structures included a ligand. Then, potential allosteric sites predicted based on the combination of hub residues and SILCS predictions were given. In addition, for each case, we performed a spectral analysis of the graphs generated by the RIN model to reveal the distinct structural domains on the receptors similar to a previous study,[56] and to show that both known and predicted binding sites are located at the interface of structural domains.

Adenosine A1 Receptor. The adenosine A1 receptor (A_1R) is a prospective pharmacological target for the treatment of neuropathic pain.[71] Developing a selective agonist and/or antagonist against the A_1R is vital in preventing any side effects associated with conserved sites. Recently, benzyloxy-cyclopentyladenosine (BnOCPA) has been discovered as an A_1R selective agonist used as an analgesic drug without inducing sedation, bradycardia, hypotension, or respiratory depression.[72] A_1R is also essential for cardiac, and renal activities, which highlights A_1R as an attractive drug target.[73]

We investigated 5 crystal structures listed in Supporting Information Table S1 involving orthosteric agonist and antagonists, and a PAM using the RIN model to determine the hub residues that have a high capacity to send and receive perturbations throughout the receptor structure. RIN was able to predict the orthosteric and allosteric binding sites with high statistical values. Similarly, SILCS-Hotspot calculations based on the crystal structure with PDB ID 7ld4 successfully found the known binding sites of A_1R (Table S2). The number of fragments engaged in the orthosteric site was up to 87 belonging to Hotspot 4 (−4.28 kcal/mol mean LGFE)

https://doi.org/10.1021/acsomega.4c06172
ACS Omega 2024, 9, 40154−40171

overlapping with selective covalent antagonist DU172, antagonist PSB36, and endogenous agonist adenosine. DU172 also overlapped with the Hotspot 54. In addition, Hotspot 2 is within 5 Å of orthosteric site ligands. From Table S2, it seems that no hub residues were detected near Hotspots 2, 4, and 54 within a distance of 5 Å. In fact, RIN was able to predict 4 true positives for both orthosteric and allosteric sites of A_1R according to the experimental dataset (Table S1). This discrepancy is due to the tight cutoff distance of 5 Å between the hub residues and Hotspots used to propose putative binding sites. For some known binding sites, also including the orthosteric binding site of A_1R, the distance between a Hotspot and a hub residue was slightly higher than 5 Å. On the other hand, Hotspots 6 and 57 with a total of 87 fragments were found next to the PAM in the protein−lipid interface. In this case, the hub residue L276 was located near Hotspot 6. These results, which are illustrated in Figure 1A, showed the success of the implemented methodology in predicting known binding sites of A_1R.

The druggability of the putative allosteric sites predicted by RIN was determined with the SILCS-Hotspots calculations for the crystal structure PDB ID 7ld4. Here, we focused on the favorable Hotspots involving a high number of fragments with high LGFE values that are within a 5 Å distance of the hub residues (Table S2). Besides the known binding sites, RIN and SILCS-Hotspots determined six putative allosteric sites mostly at the protein−lipid interface. These are shown in Figure 1A and listed in Supporting Information Table S2. Sites #1 and #2 mark two distinct cavities occupied by numerous fragments. Mean LGFE values of Hotspots 3, 41, and 42 at site #1 were −4.75, −3.05, and −3.03 kcal/mol, respectively, and the number of fragments was up to 83, all indicating the druggability of this site. Site #2 accommodates Hotspots 7, 8, and 68, with a total number of fragments of 180. Site #2 is surrounded by the hub residues L96, A100, V103, and W188 and adjacent to the highly conserved DRY motif that regulates conformational states of class A GPCRs.[74] Sites #3, and #4 are neighboring sites engaging with Hotspot 28 (mean LGFE −3.32 kcal/mol) with 62 fragments, and Hotspot 40 (mean LGFE is −3.12 kcal/mol), respectively. Another plausible allosteric drug binding site #5 faces the extracellular site, whereas site #6 is neighboring the orthosteric site of A_1R. There are other predicted sites with a low number of fragments, which may be also evaluated as potential allosteric sites (Table S2, last row). Figure 1B shows the FragMaps for A_1R obtained from the SILCS-Hotspots calculations for the putative allosteric sites #1−6. Sites #1, #3, #4, and #5 are mostly occupied with apolar fragments and a few H-bond acceptor fragments. Site #2 accommodates apolar, H-bond acceptor, and H-bond donor groups, whereas site #6 which is an embedded cavity in the receptor is dominated by H-bond donor, H-bond acceptor, negative and positive fragments.

β2-Adrenergic Receptor. β2-adrenergic receptor (β_2AR) interacts with adrenaline and is prominent in airway smooth muscles as well as cardiac and uterine muscles. It is clinically investigated for bronchial asthma and chronic obstructive pulmonary disease.[75] The protein is widely expressed with distinct densities on various immune cells, including T cells, B cells, dendritic cells (DCs), and macrophages,[76] which makes β_2AR an important target in numerous diseases. The orthosteric site of β_2AR is occupied by several agonists and antagonists, as shown by structural data (PDB IDs: 6oba, 6n48, 7dhi, 7dir, 7bz2, 6ni3, 6prz, 6ps1, 6ps3, 6ps5, 6ps0, 6ps4, 6mxt, 5x7d, 5d5b, 4qkx, 4ldo, 4ldl, 3pds). Since agonists activate all β subtypes, a selective β_2AR agonist as well as a selective antagonist have not been approved by the FDA so far,[75] and efforts to identify novel allosteric modulators for the protein are ongoing including the application of the SILCS methodology.[51]

RIN and SILCS-Hotspots predicted the orthosteric and three known allosteric sites (Supporting Information Table S1 and S3) illustrated on the β_2AR crystal structure with PDB ID 5x7d (Figure 2A). The Hotspots 20, 31, 41, 47, 55, and 67 determined by the SILCS-Hotspots calculations are located in the orthosteric pocket. The known allosteric ligand AS408, overlaps with Hotspots 1 and 12 at allosteric site 1 also accommodating the hub residues E122 and P211 from RIN. Hotspots 8 and 15 are adjacent to Cmpd-6FA at allosteric site 2. Next to allosteric site 2, Cmpd-15PA at allosteric site 3 overlaps with Hotspots 23, 58, and 60. FragMaps displayed in Figure 2B indicate that the orthosteric site of β_2AR interacts with apolar and positively charged moieties consistent with the functional groups in adrenaline and other known agonists. While allosteric site #1 is predicted to bind apolar and positively charged ligands, allosteric sites 2 and 3 are predicted to engage apolar molecules.

Calculations suggested six potential allosteric binding sites for β_2AR (Figure 2A and Table S3). Site #1 is located at the transmembrane region accessible from the intracellular site. It is marked by Hotspots 24, 36, 38, and 51 with a mean LGFE score of about −2.5 kcal/mol. Hub residue M215 on site #1 has been previously reported to undergo conformational changes in the full agonist/G protein-bound and the inverse agonist-bound forms.[77] In addition, the hub residue Y326 of the NPxxY motif is critical for receptor activation.[78] Site #1 has recently been identified as an allosteric site by SILCS calculations for β_2AR conformers generated from MD simulations as verified by *in vitro* and *ex vivo* assays.[51] Site #2 is located at the lipid−protein interface indicated by Hotspots 40 and 54, with a considerable number of fragments. Sites #3 and #4 are indicated by Hotspots 2 (mean LGFEs −3.27 kcal/mol) and 10 (mean LGFEs −2.85 kcal/mol), respectively. Although these sites are narrow accommodating a small number of fragments, they can be considered as putative allosteric sites accessible from the extracellular face. Similarly, sites #5 and #6 are occupied by a lower number of fragments. However, both sites accommodate a high number of hub residues next to motifs, such as CWxP[78] and NpxxY,[78] underlining these sites as critical. Also, M279 which assumes different conformations at different states of the receptor, similar to M215,[77] is found in sites #5 and 6. Based on the FragMaps (Figure 2B), site #1 can be targeted by H-bond donor/acceptor groups and ligands with positive or negative charge. Apolar fragments occupy site #1 as well. Site #2 is predicted to accommodate ligands containing apolar, H-bond donor, and acceptor groups. For sites #3−6, mostly apolar FragMaps are observed.

Chemokine Receptor CXCR2. CXCR2, a subtype of the chemokine receptor family expressed by neutrophils, is essential in leukocyte recruitment and integrin activation.[79] Malignancies, particularly melanoma, have autocrine activation of CXCR2.[80,81] A poor prognosis for patients is associated with overexpression of CXCR2, suggesting that CXCR2 plays a crucial role in pro-tumor actions.[80] Thus, CXCR2 is evaluated as an anticancer drug target.[82]

https://doi.org/10.1021/acsomega.4c06172
ACS Omega 2024, 9, 40154−40171

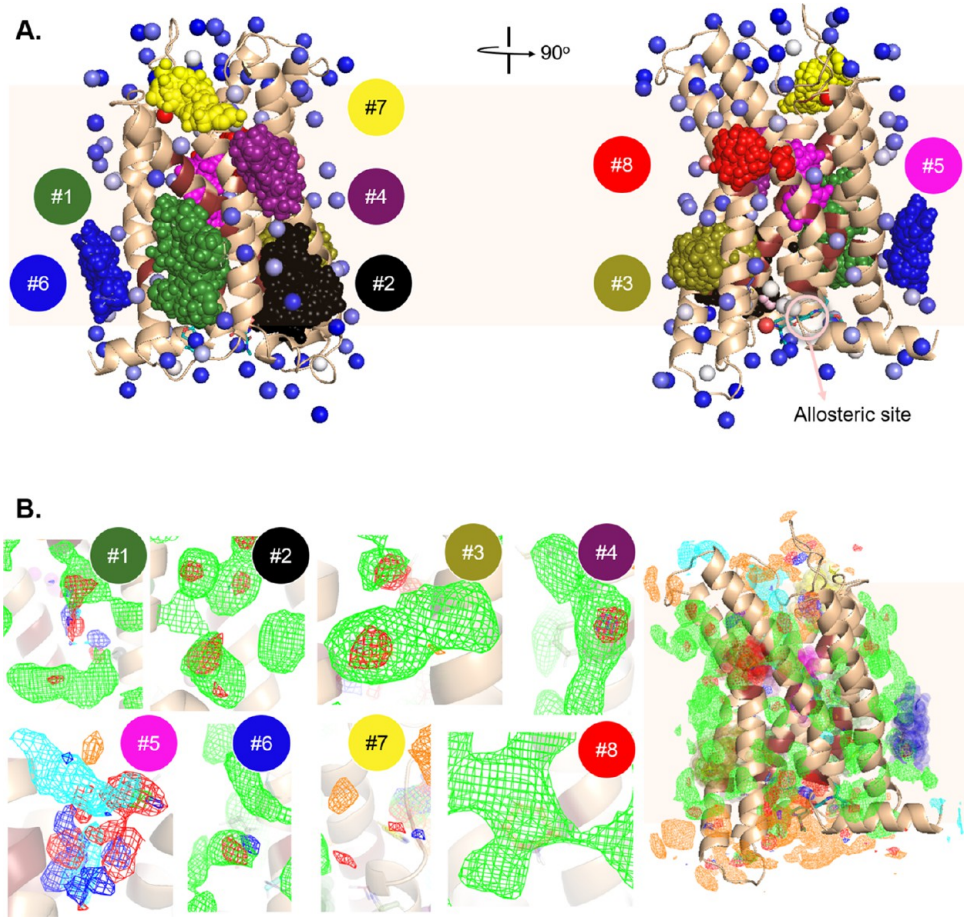

Figure 3. RIN and SILCS findings for CXCR2. (A) Structure of CXCR2 (tan cartoon) with the SILCS Hotspots (vdW spheres colored from least favorable mean LGFE (blue) to red (most favorable mean LGFE)) and the hub residues (in ruby) is shown from two perspectives. Fragments on Hotspots associated with proposed sites (#1−8) are displayed as spheres. Details of the site prediction are given in Table S4. (B) FragMaps displayed on the structure for each site in mesh, explicitly showing the generic apolar (green, −0.9 kcal/mol), generic H-bond donor (blue, −0.9 kcal/mol), generic H-bond acceptor (red, −0.9 kcal/mol), negative (orange, −1.2 kcal/mol), and positive (cyan, −1.2 kcal/mol) FragMap types.

The allosteric site of CXCR2 with the allosteric antagonist 00767013 in the intracellular region is successfully predicted by RIN using apo-structures PDB ID 6lfl, 6lfo and holo-structure PDB ID 6lfm (hub residue Y314) and SILCS-Hotspots based on the crystal structure PDB ID: 6lfl (Hotspots 94 and 15) (Figure 3A). FragMaps suggested that the intracellular region is suitable for negatively charged ligand binding (Figure 3B). On the other hand, the binding cavity of 00767013 can establish H-bonds and apolar interactions.

Eight distinct druggable sites were suggested for CXCR2 as displayed in Figure 3A and listed in Table S4. All these sites accommodate a high number of fragments, underlying the plausibility of the sites for drug targeting. Site #1, consisting of Hotspots 6 with 84 fragments and 22 with 41 fragments, is occupied by H-bond donor and acceptor groups along with apolar fragments (Figure 3B). On the other hand, site #2, with Hotspots 3 and 8 mean LGFE up to −4.39 kcal/mol, is occupied mostly by apolar FragMaps. FragMaps also predicted that molecules with apolar and H-bond acceptor moieties may bind to sites #3 and #4, occupied by Hotspots 21 and 7, respectively. Site #5 comprises toggle switch residues (F130 and W264)[83] detected as hub residues by RIN, and Hotspot 9 with 52 fragments at this particular site. Sites #6 and #8 at the protein−lipid interface, engage with apolar molecules, and #7 at the extracellular region are also promising as drug-targeting regions.

Dopamine Receptor DRD1. Dopamine receptors constitute a critical part of the central nervous system, playing roles in locomotion, cognition, and emotion.[84] Numerous clinical disorders, including hyperprolactinemia, Parkinson's, schizophrenia, Tourette syndrome, attention deficit/hyperactivity, and Huntington's syndrome, are caused by dysfunction of dopamine neurotransmission and its receptors. Especially dopamine 1 (D1) receptor is associated with memory, attention, impulse control, renal function, and locomotion.[85] Moreover, neuropsychiatric disorders and signal transduction pathways in the cell which involve phospholipase C activation and intracellular calcium release are related to D1.[85]

Calculations with RIN using 13 ligand-bound crystal structures listed in Table S1 and SILCS-Hotspots using PDB ID: 7crh predicted the orthosteric and allosteric sites of DRD1 (Figure 4 and Table S5). The orthosteric site is occupied by Hotspots 7, 11, and 24, with highly favorable mean LGFE values. DRD1 agonists retrieved from crystal structures listed in Table S1 overlap with Hotspot 24 including 66 unique fragments, while adenosine overlaps with Hotspot 7. Positive allosteric modulator LY3154207 located close to the intra-

https://doi.org/10.1021/acsomega.4c06172
ACS Omega 2024, 9, 40154−40171

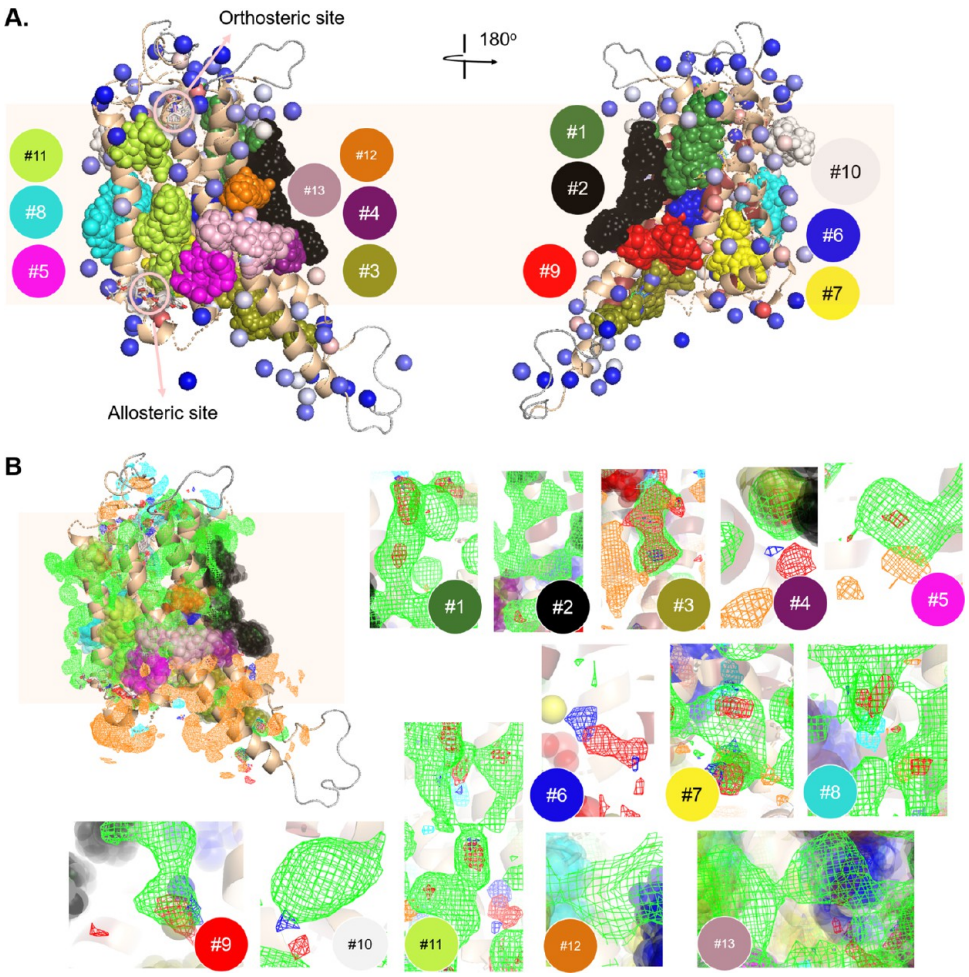

Figure 4. RIN and SILCS findings for DRD1. (A) Structure of DRD1 (tan cartoon) with the SILCS Hotspots (vdW spheres, colored from least favorable mean LGFE (blue) to red (most favorable mean LGFE)) and the hub residues (in ruby) is shown from two perspectives. Fragments on Hotspots associated with proposed sites (#1−13) are displayed as spheres. Details of the site prediction are given in Table S5. (B) FragMaps displayed on the structure for each site in mesh, explicitly showing the generic apolar (green, −0.9 kcal/mol), generic H-bond donor (blue, −0.9 kcal/mol), generic H-bond acceptor (red, −0.9 kcal/mol), negative (orange, −1.2 kcal/mol), and positive (cyan, −1.2 kcal/mol) FragMap types.

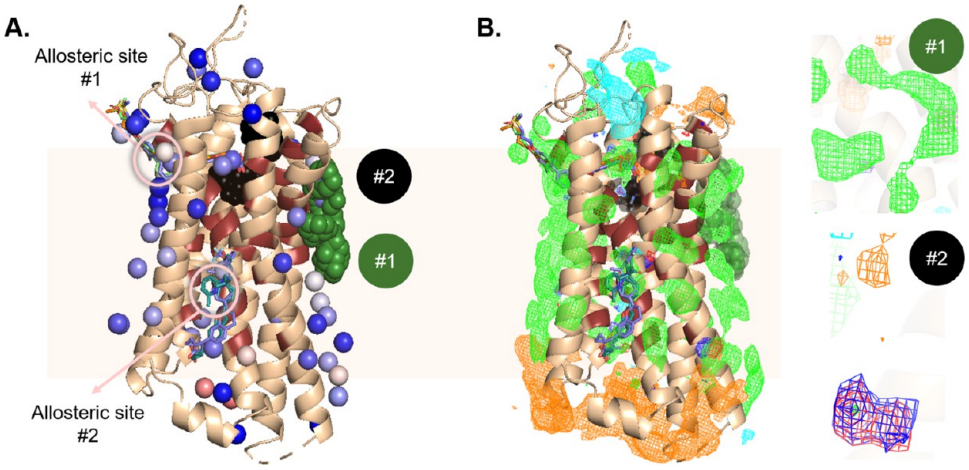

Figure 5. RIN and SILCS findings for FFA1. (A) Structure of FFA1 (tan cartoon) with the SILCS Hotspots (vdW spheres, colored from least favorable mean LGFE (blue) to red (most favorable mean LGFE)) and the hub residues (in ruby) is shown from two perspectives. Fragments on Hotspots associated with proposed sites (#1−6) are displayed as spheres. Details of the site prediction are given in Table S6. (B) FragMaps displayed on the structure for each site in mesh, explicitly showing the generic apolar (green, −0.9 kcal/mol), generic H-bond donor (blue, −0.9 kcal/mol), generic H-bond acceptor (red, −0.9 kcal/mol), negative (orange, −1.2 kcal/mol), and positive (cyan, −1.2 kcal/mol) FragMap types.

https://doi.org/10.1021/acsomega.4c06172
ACS Omega 2024, 9, 40154−40171

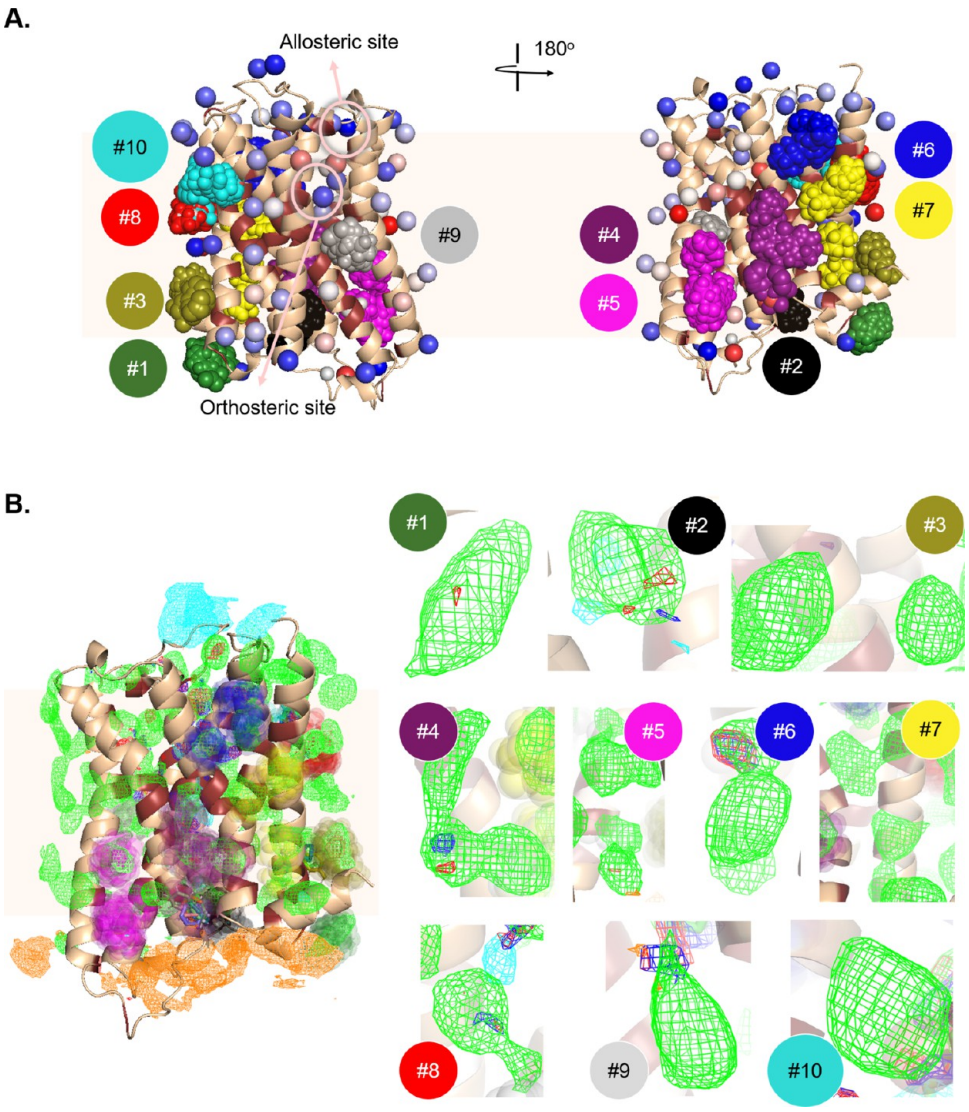

Figure 6. RIN and SILCS findings for M2. (A) Structure of M2 (tan cartoon) with the SILCS Hotspots (vdW spheres, colored from least favorable mean LGFE (blue) to red (most favorable mean LGFE)) and the hub residues (in ruby) is shown from two perspectives. Fragments on Hotspots associated with proposed sites (#1−10) are displayed as spheres. Details of the site prediction are given in Supporting Information Table S7. (B) FragMaps displayed on the structure for each site in mesh, explicitly showing the generic apolar (green, −0.9 kcal/mol), generic H-bond donor (blue, −0.9 kcal/mol), generic H-bond acceptor (red, −0.9 kcal/mol), negative (orange, −1.2 kcal/mol), and positive (cyan, −1.2 kcal/mol) FragMap types.

cellular region of DRD1 is next to Hotspots 21 and 89 and it is within 5 Å of Hotspots 10 and 105.

Ten allosteric sites are proposed for DRD1 based on Hotspot occupancy and hub residues, which are detailed in Table S5 and displayed in Figure 4A. Notably, proposed sites are populated by numerous hub residues, mostly involved in GPCR motifs that are affected by receptor activation. For instance, site #1 is indicated with Hotspots 12, 28, and 46 with a high number of fragments, and hub residues next to the NPxxY motif. Site #7 also neighbors the NPxxY motif. Another plausible site is site #2 with the hub residue V283, which is adjacent to the toggle switch residue W285. The DRY motif residue Y122 and Hotspot 50 mark site #5 as an attractive target site. Figure 4B displays the FragMaps on the structure from different perspectives. Notably, positive FragMaps are populated at the extracellular site, whereas negative FragMaps are noted for the intracellular site. With a closer look at the putative sites, mostly apolar and a small amount of H-bond donor/acceptor groups are predicted to have an affinity to sites #1, #2, #5, #8, #9, #10, and #11. Sites #3, #4, and #5, which are closer to the intracellular site bind negative fragments. Sites #12 and #13 are noted to engage apolar fragments.

Free Fatty Acid Receptor FFA1. Free fatty acid receptor (FFA1), also known as G protein-coupled receptor 40, is located in intestinal enteroendocrine cells and pancreatic β cells. It is triggered by saturated or unsaturated fatty acids, and its partial agonists have been studied for the treatment of type 2 diabetes due to regulating insulin secretion.[86] The known allosteric sites 1 and 2 of FFA1 were successfully predicted by RIN (crystal structures with PDB IDs: 4phu, 5kw2, 5tzy, 5tzr) and SILCS-Hotspots (crystal structure PDB ID: 4phu) as detailed in Table S6 and shown in Figure 5A. Allosteric site 1 is near the extracellular site and allosteric site 2 is at the transmembrane region. Calculations suggest that allosteric site 1 can bind both polar and apolar ligands while apolar ligands

https://doi.org/10.1021/acsomega.4c06172
ACS Omega 2024, 9, 40154−40171

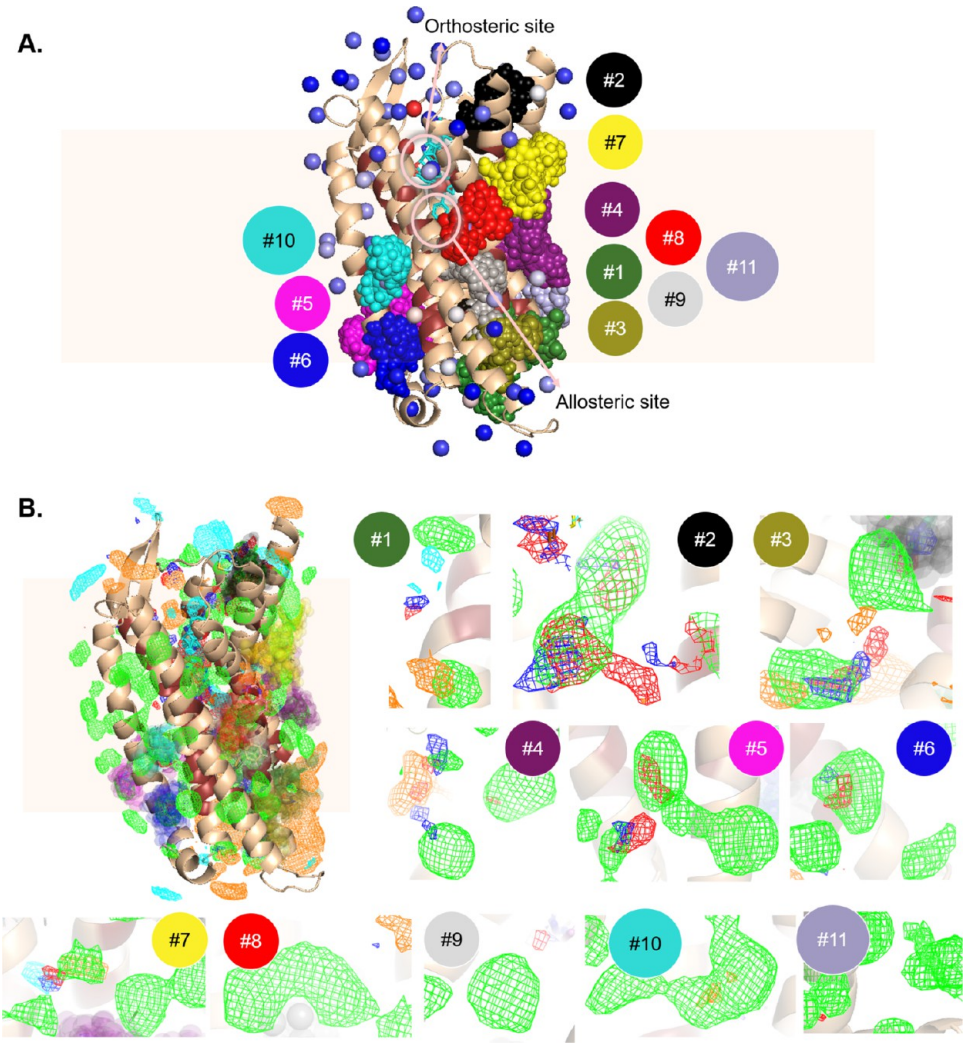

Figure 7. RIN and SILCS findings for OPRD inactive state. (A) Structure of OPRD (tan cartoon) with the SILCS Hotspots (vdW spheres, colored from least favorable mean LGFE (blue) to red (most favorable mean LGFE)) and the hub residues (in ruby) is shown from two perspectives. Fragments on Hotspots associated with proposed sites (#1−11) are displayed as spheres. Details of the site prediction are given in Table S8. (B) FragMaps displayed on the structure for each site in mesh, explicitly showing the generic apolar (green, −0.9 kcal/mol), generic H-bond donor (blue, −0.9 kcal/mol), generic H-bond acceptor (red, −0.9 kcal/mol), negative (orange, −1.2 kcal/mol), and positive (cyan, −1.2 kcal/mol) FragMap types.

are predicted to have affinity for the allosteric site 2 (Figure 5B).

The results from RIN and SILCS-Hotspots calculations indicated two plausible allosteric regions for FFA1 (Figure 5A). Site #1 is occupied by Hotspots 1, 28, and 34 with mean LGFE values changing between −4.80 and −2.50 kcal/mol, while the cumulative number of fragments engaged in site #1 is 11. On the other hand, site #2 with Hotspots 50 and 51 is adjacent to the orthosteric site of the GPCR. FragMaps indicate that site #1 can accommodate apolar ligands, whereas site #2 is appropriate for negatively charged ligands (Figure 5B).

Muscarinic Receptor Type 2. Muscarinic receptor type 2 (M2), a subtype of Muscarinic acetylcholine receptors, plays a role in heart rate and temperature regulation.[87] The smooth muscles of the airway express both M2 and M3 muscarinic receptors, with a preponderance of M2 receptors. The adrenergic system's role in mediating the relaxation of the airway smooth muscle is inhabited by activation of the M2 receptors.[88]

Here, we investigated eight crystal structures of M2 (PDB IDs: 3uon, 4mqs, 4mqt, 5yc8, 5zk3, 5zk8, 5zkb, 5zkc, 6oik, 6u1n) using RIN to calculate the hub residues with a high capacity to send and receive a perturbation. Then, the SILCS-Hotspots simulations were performed based on PDB ID 3uon. Hotspots within 5 Å of the hub residues were identified, and mean LGFE values and the number of fragments were considered to first assess the ability of this approach to find known binding sites, and then to suggest druggable allosteric sites (Table S7 and Figure 6A). RIN and SILCS successfully predicted the orthosteric site and the nearby known allosteric site at the extracellular region. SILCS Hotspots 6, 7, 45, and 64 overlap with the antagonist and agonist in the orthosteric pocket, while Hotspots 33, 61, and 77 occupy the allosteric site of M2 where LY2119620 binds. Analysis of the FragMaps indicated that a positively charged ligand is expected to have favorable interactions with the allosteric site of M2, while the orthosteric site is predicted to interact with apolar and H-bond donor/acceptor groups as well as positively charged ligands

https://doi.org/10.1021/acsomega.4c06172
ACS Omega 2024, 9, 40154−40171

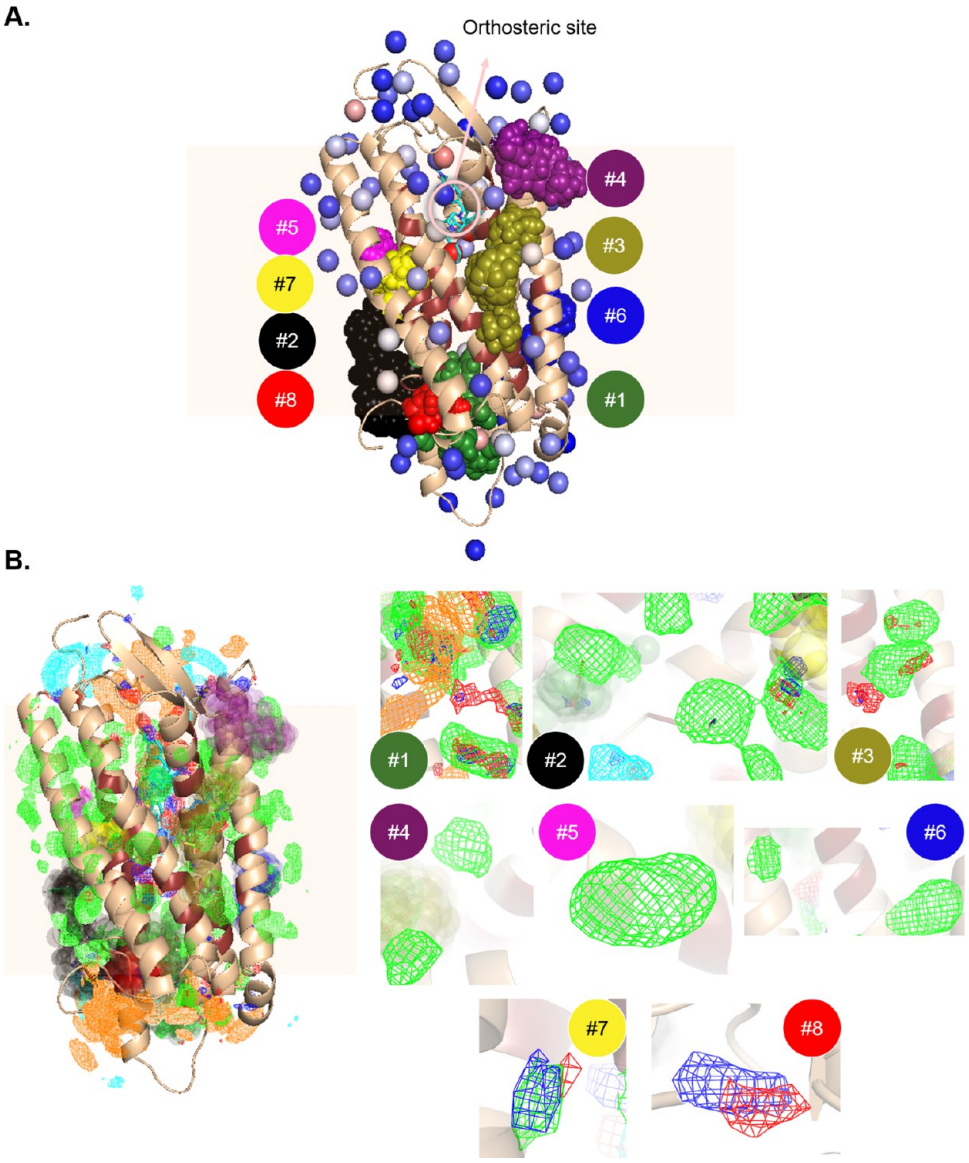

Figure 8. RIN and SILCS findings for the OPRD-active state. (A) Structure of OPRD (tan cartoon) with the SILCS Hotspots (vdW spheres, colored from least favorable mean LGFE (blue) to red (most favorable mean LGFE)) and the hub residues (in ruby) is shown from two perspectives. Fragments on Hotspots associated with proposed sites (#1−8) are displayed as spheres. Details of the site prediction are given in Table S9. (B) FragMaps displayed on the structure for each site in mesh, explicitly showing the generic apolar (green, −0.9 kcal/mol), generic H-bond donor (blue, −0.9 kcal/mol), generic H-bond acceptor (red, −0.9 kcal/mol), negative (orange, −1.2 kcal/mol), and positive (cyan, −1.2 kcal/mol) FragMap types.

(Figure 6B), consistent with the structure of muscarine and related compounds.

RIN and SILCS proposed ten putative binding sites for M2 at the intracellular region and protein−lipid interface, as shown in Figure 6A. Based on the FragMaps, apolar ligands are predicted to occupy the proposed sites located in both the intracellular region and protein−lipid interface (Figure 6B). Notably, sites #1, #3, and #4 are occupied by the highest number of fragments associated with fragments 50 and 83. Site #2 in the intracellular region of M2 is occupied by Hotspot 9 with 30 fragments. Hotspots 20 and 54, of which the cumulative fragments amounted to 41, reside in site #5. Sites #6 and #7 at the protein−lipid interface are adjacent to TM2 and TM7. While site #6 contains Hotspots 3, 4, 26, and 51, Hotspots 13, 30, 34, and 52 are located in site #7. Notably, site #7 contains NPxxY motif residues P437 and Y440. Sites #8, #9 and #10 at the lipid−protein interface are each occupied by a total of 25, 15, and 21 fragments, respectively.

δ-Opioid Receptor. OPRD is a target for the treatment of neurological and psychiatric disorders,[89] as well as chronic pain.[90] The structural motifs of the opioid receptors are largely conserved, despite poor sequence conservation.[91] The orthosteric regions containing agonists and antagonists are indicated by the crystal structures of the δ-opioid receptor (PDB IDs: 4ej4, 4rwa, 4rwd, 6pt3, 8f7s, 4n6h, 6pt2), where the active and inactive conformers were available for the calculations. In the inactive conformer, $OPRD_{inactive}$, the orthosteric antagonist Naltrindole overlaps with Hotspot 5, while it is adjacent to Hotspot 41 (Figure 7A and Supporting Information Table S8).[52] The binding region of another peptide antagonist, DIPP-NH2, is near the Hotspots 1, 3, 5, and the Hotspots 11 and 41 together with the hub residues

https://doi.org/10.1021/acsomega.4c06172
ACS Omega 2024, 9, 40154−40171

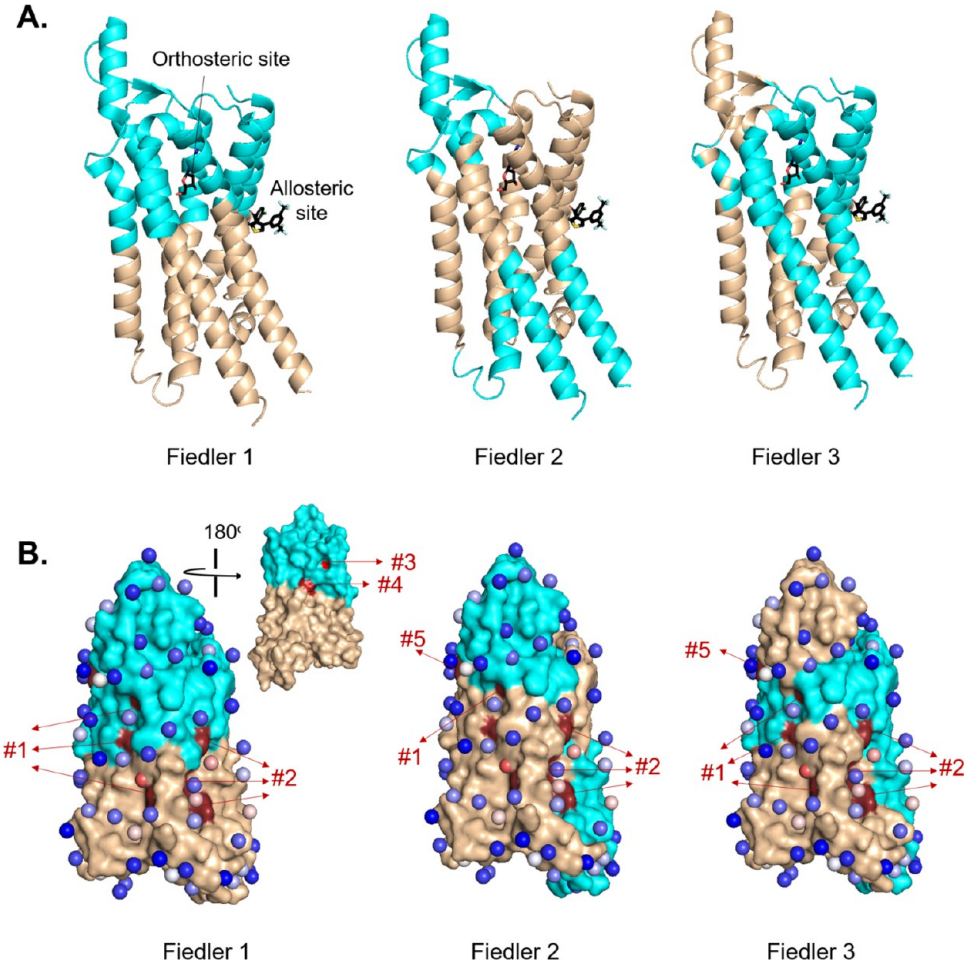

Figure 9. Distinct structural domains of A_1R from nonzero Fiedler vectors 1, 2, and 3, are shown in cyan and wheat. (A) The positions of the known binding sites are indicated by the ligands from the crystal structure (PDB ID: 7ld3). (B) Predicted sites are displayed by the hub residues (in firebrick surface) and the Hotspots (in spheres) along with their numbering given in Table S2.

V217 and H301. Moreover, SILCS and RIN calculations detected the Na^+ binding pocket as one of the most druggable sites, marked by Hotspots 1 and 2 with highly favorable LGFE values. It is worth noting that hub residue W274 is located at the Na^+ binding pocket, and is part of the CWxP motif.[92] In addition, at the orthosteric binding site hub residue F270 of the PIF motif[92] was found by the calculations. Based on FragMaps (Figure 7B), the Na^+ binding pocket has a predicted affinity for positively charged ligands, as expected. On the other hand, a variety of FragMaps was observed to bind the orthosteric site, including H-bond donor/acceptor, positive and negative maps as well as apolar FragMaps. This is consistent with the wide range of different classes of molecules that interact with the opioid receptors.[93,94]

Calculations suggested ten allosteric binding sites for $OPRD_{inactive}$ shown on the crystal structure PDB ID: 4ej4 in Figure 7A and detailed in Supporting Information Table S8. The majority of the sites are near the intracellular region. For example, site #1, easily accessible from the intracellular region, involves the hub residues I259, M262, and L321 and Hotspots 54, 78, and 86. Sites #3, 5, and 6 were also detected in the intracellular region. Particularly, site #6 is engaged with Hotspot 16, and accommodates the DRY motif hub residue D145. Here, 39 unique ring fragments of which the mean LGFE is −3.35 kcal/mol bind site #6. Site #2 can be accessed from the extracellular region and is close to the orthosteric pocket, paving the way to design bitopic ligands for OPRD. The number of fragments is 89 with a mean LGFE of −3.96 kcal/mol which highlights this site as highly druggable. Sites #4 and 7 neighboring each other are located at the protein−lipid interface. In the vicinity of site #4, Hotspots 13 and 19 reside, whereas site #7 is occupied by Hotspots 25 and 36. Site 4 is also adjacent to site #11, which is occupied by Hotspots 17 and 87, with 14 and 18 fragments, respectively. Sites #8, #9, and #10 have fewer fragments than other proposed sites. Nonetheless, these sites accommodate a high number of hub residues, which makes them interesting. FragMaps results are shown for each suggested site in Figure 7B. Here, various chemical moieties are noted to have affinity to sites #1−7 whereas only apolar fragments bound sites #8−11.

In addition, the active conformer of the receptor, $OPRD_{active}$, was studied by RIN to propose hub residues based on this contact topology, which is slightly different from the inactive state. The active conformer modeled from 6pt3.pdb in our previous study[52] was also investigated using the SILCS-Hotspots calculations. OPRD agonists, KGCHM07 and DPI-287 overlapped with the location of Hotspots 1 and 2 in the active conformer (Table S9). DPI-287 is adjacent to Hotspots 11 and 71 as well. In addition, Hotspot 27, involving 57 ring fragments, is located in the vicinity of the orthosteric site. Similar to findings for $OPRD_{inactive}$, SILCS-Hotspots and RIN point to the intracellular region of $OPRD_{active}$ as highly

https://doi.org/10.1021/acsomega.4c06172
ACS Omega 2024, 9, 40154−40171

druggable (Figure 8A). Site #1 is composed of Y233, I259, and M262, and Hotspots 3, 6, and 8 with mean LGFE down to −4.25 kcal/mol. Hotspot 8 has the highest number of 88 unique fragments, while Hotspot 3 is engaged with 11 fragments. Both mean LGFE values, a high number of fragments, and different types of fragments (Figure 8B) indicated site #1 as highly druggable. Site #2 (Hotspots 20, 35, 44; hub residues M262, V265, L321) is neighboring site #1 and promises another attractive binding site with a high number of fragments up to 84. Site #3 is located at the protein−lipid interface and can be evaluated as a putative binding site. Here, numerous hub residues as well as Hotspots 10, 15, 24, and 58, with mean LGFE values of −3.73 to −2.76 kcal/mol, are located. Site #4 accommodating the hub residue K122 is located at the extracellular region of $OPRD_{active}$ and is occupied by Hotspot 98 of which the fragment number is 24. Other sites #5 to #8 seem to be relatively less druggable due to their low number of fragments; nonetheless, fragments with H-bond donor or acceptor groups are predicted to have an affinity for sites #7 and #8 (Figure 8B).

Graph Spectral Analysis. The topology of the seven case studies, i.e., A_1R, β_2AR (active and inactive), CXCR2, DRD1, FFA1, M2, and OPRD (active and inactive), was decomposed into residue clusters, or structural domains, with graph spectral analysis. Here, the first three nonzero Fiedler vectors were considered to determine the domains formed based on the neighboring of the residues. Hotspots from SILCS simulations were then superposed on the decomposed structures. We noted a pattern, where the known orthosteric and allosteric binding sites, hub residues together with the favorable Hotspots were aligned along the structural domain interfaces indicated by the first three nonzero Fiedler vectors. These structural domains are formed by close-neighboring nodes that are expected to move together in low-frequency motions similar to the dynamic domains from the Gaussian Network Model.[27] The spectral analysis seems to reveal highly connected residues that tend to move as a rigid domain during the functional dynamics of the protein. Consequently, the interfaces of the structural domains indicated by spectral analysis have a high potential to act as hinge regions to coordinate global motions and, consequently, may participate in allosteric control.

Figure 9 shows the results for the A_1R. Domains are distinguished by different colors for each vector. The orthosteric and allosteric binding sites of A_1R are at the domain interfaces (Figure 9A). The same observation was also made for the other investigated structures, shown in Figures S19A−S25A. Moreover, we also noted that the domain interfaces pass through or are aligned along the hub residues of proposed sites (Figure 9B) accommodating numerous fragments as listed in Table S2. For instance, hub residue L90 and Hotspot 41 of site #1, hub residues L96, W188, and Hotspot 7 of site #2, and hub residue L276 and Hotspot 40 of site #4, reside along the structural domain interfaces of Fiedler vector 1. Site #4 indicated by the hub residue L276 and Hotspot 40 is at the domain interface detected by Fiedler vector 1. On the other hand, spectral analysis from Fiedler vector 2 indicated hub residue C85-Hotspot 42 (site #1), and hub residues L96, W188 - Hotspots 7 and 68 (site #2) at the domain interface. Sites #1 and #2 were also observed on the domain interfaces of Fiedler vector 3. In addition, hub residue I71 - Hotspot 82 of site #5 is located at the domain interface of Fiedler vectors 2 and 3. The consistency of the graph spectral analysis with the RIN results suggested that the binding of a compound at a domain interface has a high potential to allosterically modulate the conformational dynamics of the receptor and thereby impact biological activity.

Similarly, for the other structures, the first three nonzero Fiedler vectors from the graph spectral analysis reveal that the proposed allosteric sites accumulate on the domain interfaces, making our predictions highly plausible. Domain decompositions for the structures are displayed in Figures S19B−S25B, where the indicated sites can be found in more detail in Tables S2−S9.

CONCLUSIONS

Analysis of a collection of well-characterized proteins with multiple known ligands indicated that the RIN model can successfully predict known binding sites of class A GPCRs by determining the hub residues of the network constructed based on contact topology. The druggability of hub residues for 7 distinct class A GPCRs, namely adenosine A1 receptor, β2-adrenergic receptor, chemokine receptor CXCR2, dopamine receptor D1, free fatty acid receptor, muscarinic receptor type 2 (M2), and δ-opioid receptor, was then evaluated with the SILCS-Hotspots technology. It was shown that known ligand-binding sites were found at the mutual sites marked by the hub residues and by the frequently sampled SILCS Hotspots. Moreover, the mutual sites were located at the interfaces of highly interconnected nodes according to the graph spectral analysis. The node clusters seemed to form large domains with an ability to move collectively, as in a functional hinge motion. Thus, the domain interfaces can provide strategical spots to design allosteric modulators. Finally, numerous putative allosteric binding sites, remote from the orthosteric sites were proposed for the 7 class A GPCRs, which are highly critical in various diseases. The computational approach presented here combines the key topological properties of the protein structure and the detailed fragment-based mapping and can serve as a highly useful tool to explore allosteric binding regions of proteins and their complexes. To further improve the predictions in exploring best binding sites, developing a metric using rank-ordering can be beneficial. However, this necessitates careful validation through a large dataset, such as that applied during the development of a recently improved ranking of the SILCS Hotspots using a machine-learning model.[95]

ASSOCIATED CONTENT

Data Availability Statement

The crystallographic structures are available from https://www.rcsb.org. The SILCS software suite is available at no charge to academic users from SilcsBio LLC (http://www.silcsbio.com). Molecular graphics are generated with the free software PyMOL (DeLano Scientific LLC, 2002). The data underlying this study are available in the published article and its Supporting Information.

Supporting Information

The Supporting Information is available free of charge at https://pubs.acs.org/doi/10.1021/acsomega.4c06172.

Table S1. Statistical analysis for the binding site prediction ability of the residue interaction network model (RIN); **Tables S2−S8**. Predicted binding sites for A_1R, β_2AR; CXCR2; DRD1; FFA1; M2; OPRD-inactive; and OPRD-active proteins using RIN and

https://doi.org/10.1021/acsomega.4c06172
ACS Omega 2024, 9, 40154−40171

SILCS-Hotspots; **Figures S1−S18**. Z-scores for the hub residues predicted using RIN for the dataset of 18 class A GPCR structures; **Figures S19−S25**. Graph spectral analysis for β_2AR; CXCR2; DRD1; FFA1; M2; OPRD-inactive; and OPRD-active proteins (PDF)

AUTHOR INFORMATION

Corresponding Authors

Alexander D. MacKerell, Jr. − *University of Maryland Computer-Aided Drug Design Center, Department of Pharmaceutical Sciences, School of Pharmacy, University of Maryland, Baltimore, Maryland 21201, United States;* orcid.org/0000-0001-8287-6804; Email: alex@outerbanks.umaryland.edu

Ozge Kurkcuoglu − *Department of Chemical Engineering, Istanbul Technical University, Istanbul 34469, Turkey;* orcid.org/0000-0003-0228-3211; Phone: +90 2122853523; Email: olevitas@itu.edu.tr; Fax: +90 2122853425

Authors

Tugce Inan − *Department of Chemical Engineering, Istanbul Technical University, Istanbul 34469, Turkey; Chemical Engineering Department, Faculty of Engineering & Architecture, Istanbul Beykent University, Istanbul 34396, Turkey;* orcid.org/0000-0002-4762-713X

Merve Yuce − *Department of Chemical Engineering, Istanbul Technical University, Istanbul 34469, Turkey*

Complete contact information is available at: https://pubs.acs.org/10.1021/acsomega.4c06172

Author Contributions

‖T.I. and M.Y. contributed equally to this work. All authors contributed to the study conception and workflow. T.I. and M.Y. performed the residue interaction network calculations and analysis. M.Y. performed the statistical analysis. A.D.M., Jr., performed SILCS calculations. The manuscript was written through the contributions of all authors. All authors have approved the final version of the manuscript.

Notes

The authors declare the following competing financial interest(s): ADM Jr., is co-founder and CSO of SilcsBio LLC. The other authors declare no competing financial interest.

ACKNOWLEDGMENTS

Computing resources used in this work were provided by the National Center for High Performance Computing of Turkey (UHeM), the TÜBİTAK ULAKBİM High Performance and Grid Computing Center (TRUBA), and the University of Maryland Computer-Aided Drug Design Center. M.Y. thanks to the TUBITAK National Ph.D. Scholarship Program in the Priority Fields in Science and Technology (2211/C). O.K. acknowledges Istanbul Technical University Scientific Project THD-2024-45545 and TDK-2020-42717 and A.D.M., Jr., acknowledges support from the NIH (R35 GM131710).

REFERENCES

(1) Insel, P. A.; Sriram, K.; Gorr, M. W.; Wiley, S. Z.; Michkov, A.; Salmerón, C.; Chinn, A. M. GPCRomics: An Approach to Discover GPCR Drug Targets. *Trends Pharmacol. Sci.* **2019**, *40* (6), 378−387.

(2) Sriram, K.; Insel, P. A. G Protein-Coupled Receptors as Targets for Approved Drugs: How Many Targets and How Many Drugs? *Mol. Pharmacol.* **2018**, *93* (4), 251−258.

(3) Wold, E. A.; Zhou, J. GPCR Allosteric Modulators: Mechanistic Advantages and Therapeutic Applications. *CTMC* **2019**, *18* (23), 2002−2006.

(4) Yang, D.; Zhou, Q.; Labroska, V.; Qin, S.; Darbalaei, S.; Wu, Y.; Yuliantie, E.; Xie, L.; Tao, H.; Cheng, J.; Liu, Q.; Zhao, S.; Shui, W.; Jiang, Y.; Wang, M.-W. G Protein-Coupled Receptors: Structure- and Function-Based Drug Discovery. *Signal Transduction Targeted Ther.* **2021**, *6* (1), No. 7.

(5) Allegretti, M.; Cesta, M. C.; Locati, M. Allosteric Modulation of Chemoattractant Receptors. *Front. Immunol.* **2016**, *7*, No. 170.

(6) Zou, R.; Wang, X.; Li, S.; Chan, H. C. S.; Vogel, H.; Yuan, S. The Role of Metal Ions in G Protein-coupled Receptor Signalling and Drug Discovery. *WIREs Comput. Mol. Sci.* **2022**, *12* (2), No. e1565.

(7) Mosi, R. M.; Anastassova, V.; Cox, J.; Darkes, M. C.; Idzan, S. R.; Labrecque, J.; Lau, G.; Nelson, K. L.; Patel, K.; Santucci, Z.; Wong, R. S. Y.; Skerlj, R. T.; Bridger, G. J.; Huskens, D.; Schols, D.; Fricker, S. P. The Molecular Pharmacology of AMD11070: An Orally Bioavailable CXCR4 HIV Entry Inhibitor. *Biochem. Pharmacol.* **2012**, *83* (4), 472−479.

(8) Grover, A. K. Use of Allosteric Targets in the Discovery of Safer Drugs. *Med. Princ. Pract.* **2013**, *22* (5), 418−426.

(9) Mohr, K.; Schmitz, J.; Schrage, R.; Tränkle, C.; Holzgrabe, U. Molecular Alliance—From Orthosteric and Allosteric Ligands to Dualsteric/Bitopic Agonists at G Protein Coupled Receptors. *Angew. Chem., Int. Ed* **2013**, *52* (2), 508−516.

(10) Pándy-Szekeres, G.; Caroli, J.; Mamyrbekov, A.; Kermani, A. A.; Keserű, G. M.; Kooistra, A. J.; Gloriam, D. E. GPCRdb in 2023: State-Specific Structure Models Using AlphaFold2 and New Ligand Resources. *Nucleic Acids Res.* **2023**, *51* (D1), D395−D402.

(11) Kooistra, A. J.; Mordalski, S.; Pándy-Szekeres, G.; Esguerra, M.; Mamyrbekov, A.; Munk, C.; Keserű, G. M.; Gloriam, D. E. GPCRdb in 2021: Integrating GPCR Sequence, Structure and Function. *Nucleic Acids Res.* **2021**, *49* (D1), D335−D343.

(12) Daily, M. D.; Upadhyaya, T. J.; Gray, J. J. Contact Rearrangements Form Coupled Networks from Local Motions in Allosteric Proteins. *Proteins* **2008**, *71* (1), 455−466.

(13) Feher, V. A.; Durrant, J. D.; Van Wart, A. T.; Amaro, R. E. Computational Approaches to Mapping Allosteric Pathways. *Curr. Opin. Struct. Biol.* **2014**, *25*, 98−103.

(14) Kannan, N.; Vishveshwara, S. Identification of Side-Chain Clusters in Protein Structures by a Graph Spectral Method 1 1Edited by J. M. Thornton. *J. Mol. Biol.* **1999**, *292* (2), 441−464.

(15) Lockless, S. W.; Ranganathan, R. Evolutionarily Conserved Pathways of Energetic Connectivity in Protein Families. *Science* **1999**, *286* (5438), 295−299.

(16) Di Paola, L.; Giuliani, A. Protein Contact Network Topology: A Natural Language for Allostery. *Curr. Opin. Struct. Biol.* **2015**, *31*, 43−48.

(17) Brinda, K. V.; Vishveshwara, S. A Network Representation of Protein Structures: Implications for Protein Stability. *Biophys. J.* **2005**, *89* (6), 4159−4170.

(18) Kürkçüoğlu, Ö. Exploring Allosteric Communication in Multiple States of the Bacterial Ribosome Using Residue Network Analysis. *Turk. J. Biol.* **2018**, *42* (5), 392−404.

(19) Atilgan, A. R.; Durell, S. R.; Jernigan, R. L.; Demirel, M. C.; Keskin, O.; Bahar, I. Anisotropy of Fluctuation Dynamics of Proteins with an Elastic Network Model. *Biophys. J.* **2001**, *80* (1), 505−515.

(20) Haliloglu, T.; Seyrek, E.; Erman, B. Prediction of Binding Sites in Receptor-Ligand Complexes with the Gaussian Network Model. *Phys. Rev. Lett.* **2008**, *100* (22), No. 228102.

(21) Acar, B.; Rose, J.; Aykac Fas, B.; Ben-Tal, N.; Lewinson, O.; Haliloglu, T. Distinct Allosteric Networks Underlie Mechanistic Speciation of ABC Transporters. *Structure* **2020**, *28* (6), 651−663.e5.

(22) Altintel, B.; Acar, B.; Erman, B.; Haliloglu, T. Subsets of Slow Dynamic Modes Reveal Global Information Sources as Allosteric Sites. *J. Mol. Biol.* **2022**, *434* (17), No. 167644.

(23) Ciftci, H.; Tateishi, H.; Koiwai, K.; Koga, R.; Anraku, K.; Monde, K.; Dağ, Ç.; Destan, E.; Yuksel, B.; Ayan, E.; Yildirim, G.; Yigin, M.; Ertem, F. B.; Shafiei, A.; Guven, O.; Besler, S. O.; Sierra, R. G.; Yoon, C. H.; Su, Z.; Liang, M.; Acar, B.; Haliloglu, T.; Otsuka, M.; Yumoto, F.; Fujita, M.; Senda, T.; DeMirci, H. Structural Insight into Host Plasma Membrane Association and Assembly of HIV-1 Matrix Protein. *Sci. Rep* **2021**, *11* (1), No. 15819.
(24) Haliloglu, T.; Bahar, I. Adaptability of Protein Structures to Enable Functional Interactions and Evolutionary Implications. *Curr. Opin. Struct. Biol.* **2015**, *35*, 17−23.
(25) Zhang, Y.; Doruker, P.; Kaynak, B.; Zhang, S.; Krieger, J.; Li, H.; Bahar, I. Intrinsic Dynamics Is Evolutionarily Optimized to Enable Allosteric Behavior. *Curr. Opin. Struct. Biol.* **2020**, *62*, 14−21.
(26) Greener, J. G.; Sternberg, M. J. AlloPred: Prediction of Allosteric Pockets on Proteins Using Normal Mode Perturbation Analysis. *BMC Bioinf.* **2015**, *16* (1), No. 335.
(27) Kurkcuoglu, O.; Gunes, M. U.; Haliloglu, T. Local and Global Motions Underlying Antibiotic Binding in Bacterial Ribosome. *J. Chem. Inf. Model.* **2020**, *60*, 6447.
(28) Schueler-Furman, O.; Wodak, S. J. Computational Approaches to Investigating Allostery. *Curr. Opin. Struct. Biol.* **2016**, *41*, 159−171.
(29) Liu, J.; Nussinov, R. Allostery: An Overview of Its History, Concepts, Methods, and Applications. *PLoS Comput. Biol.* **2016**, *12* (6), No. e1004966.
(30) Tian, W.; Chen, C.; Lei, X.; Zhao, J.; Liang, J. CASTp 3.0: Computed Atlas of Surface Topography of Proteins. *Nucleic Acids Res.* **2018**, *46* (W1), W363−W367.
(31) Mandal, N.; Surpeta, B.; Brezovsky, J. Reinforcing Tunnel Network Exploration in Proteins Using Gaussian Accelerated Molecular Dynamics. *J. Chem. Inf. Model.* **2024**, *64* (16), 6623−6635.
(32) Brenke, R.; Kozakov, D.; Chuang, G.-Y.; Beglov, D.; Hall, D.; Landon, M. R.; Mattos, C.; Vajda, S. Fragment-Based Identification of Druggable 'Hot Spots' of Proteins Using Fourier Domain Correlation Techniques. *Bioinformatics* **2009**, *25* (5), 621−627.
(33) Kozakov, D.; Grove, L. E.; Hall, D. R.; Bohnuud, T.; Mottarella, S. E.; Luo, L.; Xia, B.; Beglov, D.; Vajda, S. The FTMap Family of Web Servers for Determining and Characterizing Ligand-Binding Hot Spots of Proteins. *Nat. Protoc.* **2015**, *10* (5), 733−755.
(34) Ivetac, A.; Andrew McCammon, J. Mapping the Druggable Allosteric Space of G-Protein Coupled Receptors: A Fragment-Based Molecular Dynamics Approach. *Chem. Biol. Drug Des.* **2010**, *76* (3), 201−217.
(35) Kumar, A.; Kaynak, B. T.; Dorman, K. S.; Doruker, P.; Jernigan, R. L. Predicting Allosteric Pockets in Protein Biological Assemblages. *Bioinformatics* **2023**, *39* (5), No. btad275.
(36) Ghanakota, P.; Carlson, H. A. Moving Beyond Active-Site Detection: MixMD Applied to Allosteric Systems. *J. Phys. Chem. B* **2016**, *120* (33), 8685−8695.
(37) Bakan, A.; Nevins, N.; Lakdawala, A. S.; Bahar, I. Druggability Assessment of Allosteric Proteins by Dynamics Simulations in the Presence of Probe Molecules. *J. Chem. Theory Comput.* **2012**, *8* (7), 2435−2447.
(38) Graham, S. E.; Leja, N.; Carlson, H. A. MixMD Probeview: Robust Binding Site Prediction from Cosolvent Simulations. *J. Chem. Inf. Model.* **2018**, *58* (7), 1426−1433.
(39) Kalenkiewicz, A.; Grant, B.; Yang, C.-Y. Enrichment of Druggable Conformations from Apo Protein Structures Using Cosolvent-Accelerated Molecular Dynamics. *Biology* **2015**, *4* (2), 344−366.
(40) Mahmoud, A. H.; Yang, Y.; Lill, M. A. Improving Atom-Type Diversity and Sampling in Cosolvent Simulations Using λ-Dynamics. *J. Chem. Theory Comput.* **2019**, *15* (5), 3272−3287.
(41) Alvarez-Garcia, D.; Barril, X. Molecular Simulations with Solvent Competition Quantify Water Displaceability and Provide Accurate Interaction Maps of Protein Binding Sites. *J. Med. Chem.* **2014**, *57* (20), 8530−8539.
(42) Lee, J. Y.; Krieger, J. M.; Li, H.; Bahar, I. Pharmmaker: Pharmacophore Modeling and Hit Identification Based on Druggability Simulations. *Protein Sci.* **2020**, *29* (1), 76−86.
(43) Lakkaraju, S. K.; Raman, E. P.; Yu, W.; Mackerell, A. D. Sampling of Organic Solutes in Aqueous and Heterogeneous Environments Using Oscillating Excess Chemical Potentials in Grand Canonical-like Monte Carlo-Molecular Dynamics Simulations. *J. Chem. Theory Comput.* **2014**, *10* (6), 2281−2290.
(44) Raman, E. P.; Yu, W.; Lakkaraju, S. K.; Mackerell, A. D. Inclusion of Multiple Fragment Types in the Site Identification by Ligand Competitive Saturation (SILCS) Approach. *J. Chem. Inf. Model.* **2013**, *53* (12), 3384−3398.
(45) MacKerell, A. D.; Jo, S.; Lakkaraju, S. K.; Lind, C.; Yu, W. Identification and Characterization of Fragment Binding Sites for Allosteric Ligand Design Using the Site Identification by Ligand Competitive Saturation Hotspots Approach (SILCS-Hotspots). *Biochim. Biophys. Acta, Gen. Subj.* **2020**, *1864* (4), No. 129519.
(46) Yu, W.; Lakkaraju, S. K.; Raman, E. P.; Fang, L.; MacKerell, A. D. Pharmacophore Modeling Using Site-Identification by Ligand Competitive Saturation (SILCS) with Multiple Probe Molecules. *J. Chem. Inf. Model.* **2015**, *55* (2), 407−420.
(47) Inan, T.; Flinko, R.; Lewis, G. K.; MacKerell, A. D.; Kurkcuoglu, O. Identifying and Assessing Putative Allosteric Sites and Modulators for CXCR4 Predicted through Network Modeling and Site Identification by Ligand Competitive Saturation. *J. Phys. Chem. B* **2024**, *128* (21), 5157−5174.
(48) Berman, H. M. The Protein Data Bank. *Nucleic Acids Res.* **2000**, *28* (1), 235−242.
(49) Isberg, V.; Mordalski, S.; Munk, C.; Rataj, K.; Harpsøe, K.; Hauser, A. S.; Vroling, B.; Bojarski, A. J.; Vriend, G.; Gloriam, D. E. GPCRdb: An Information System for G Protein-Coupled Receptors. *Nucleic Acids Res.* **2016**, *44* (D1), D356−D364.
(50) Webb, B.; Sali, A. Comparative Protein Structure Modeling Using MODELLER. *Curr. Protoc. Bioinf.* **2016**, *54* (1), 54:5.6.1−5.6.37.
(51) Shah, S. D.; Lind, C.; De Pascali, F.; Penn, R. B.; MacKerell, A. D.; Deshpande, D. A. In Silico Identification of a β_2-Adrenoceptor Allosteric Site That Selectively Augments Canonical β_2 AR-Gs Signaling and Function. *Proc. Natl. Acad. Sci. U.S.A.* **2022**, *119* (49), No. e2214024119.
(52) Olson, K. M.; Devereaux, A. L.; Chatterjee, P.; Saldaña-Shumaker, S. L.; Shafer, A.; Plotkin, A.; Kandasamy, R.; MacKerell, A. D.; Traynor, J. R.; Cunningham, C. W. Nitro-Benzylideneoxymorphone, a Bifunctional Mu and Delta Opioid Receptor Ligand with High Mu Opioid Receptor Efficacy. *Front. Pharmacol.* **2023**, *14*, No. 1230053.
(53) Fokas, A. S.; Cole, D. J.; Ahnert, S. E.; Chin, A. W. Residue Geometry Networks: A Rigidity-Based Approach to the Amino Acid Network and Evolutionary Rate Analysis. *Sci. Rep.* **2016**, *6* (August), No. 33213.
(54) Guzel, P.; Kurkcuoglu, O. Identification of Potential Allosteric Communication Pathways between Functional Sites of the Bacterial Ribosome by Graph and Elastic Network Models. *Biochim. Biophys. Acta, Gen. Subj.* **2017**, *1861* (12), 3131−3141.
(55) Yuce, M.; Cicek, E.; Inan, T.; Dag, A. B.; Kurkcuoglu, O.; Sungur, F. A. Repurposing of FDA-Approved Drugs against Active Site and Potential Allosteric Drug-Binding Sites of COVID-19 Main Protease. *Proteins* **2021**, *89* (11), 1425−1441.
(56) Halder, A.; Anto, A.; Subramanyan, V.; Bhattacharyya, M.; Vishveshwara, S.; Vishveshwara, S. Surveying the Side-Chain Network Approach to Protein Structure and Dynamics: The SARS-CoV-2 Spike Protein as an Illustrative Case. *Front. Mol. Biosci.* **2020**, *7*, No. 596945.
(57) Lakkaraju, S. K.; Yu, W.; Raman, E. P.; Hershfeld, A. V.; Fang, L.; Deshpande, D. A.; Mackerell, A. D. Mapping Functional Group Free Energy Patterns at Protein Occluded Sites: Nuclear Receptors and g-Protein Coupled Receptors. *J. Chem. Inf. Model.* **2015**, *55* (3), 700−708.
(58) Ustach, V. D.; Lakkaraju, S. K.; Jo, S.; Yu, W.; Jiang, W.; Mackerell, A. D. Optimization and Evaluation of Site-Identification by Ligand Competitive Saturation (SILCS) as a Tool for Target-Based Ligand Optimization. *J. Chem. Inf. Model.* **2019**, *59* (6), 3018−3035.

https://doi.org/10.1021/acsomega.4c06172
ACS Omega 2024, 9, 40154−40171

(59) Huang, J.; Rauscher, S.; Nawrocki, G.; Ran, T.; Feig, M.; De Groot, B. L.; Grubmüller, H.; MacKerell, A. D. CHARMM36m: An Improved Force Field for Folded and Intrinsically Disordered Proteins. *Nat. Methods* **2017**, *14* (1), 71−73.
(60) Jo, S.; Kim, T.; Iyer, V. G.; Im, W. CHARMM-GUI: A Web-Based Graphical User Interface for CHARMM. *J. Comput. Chem.* **2008**, *29* (11), 1859−1865.
(61) Van Der Spoel, D.; Lindahl, E.; Hess, B.; Groenhof, G.; Mark, A. E.; Berendsen, H. J. C. GROMACS: Fast, Flexible, and Free. *J. Comput. Chem.* **2005**, *26* (16), 1701−1718.
(62) Abraham, M. J.; Murtola, T.; Schulz, R.; Páll, S.; Smith, J. C.; Hess, B.; Lindah, E. Gromacs: High Performance Molecular Simulations through Multi-Level Parallelism from Laptops to Supercomputers. *SoftwareX* **2015**, *1−2*, 19−25.
(63) Vanommeslaeghe, K.; Hatcher, E.; Acharya, C.; Kundu, S.; Zhong, S.; Shim, J.; Darian, E.; Guvench, O.; Lopes, P.; Vorobyov, I.; Mackerell, A. D. CHARMM General Force Field: A Force Field for Drug-like Molecules Compatible with the CHARMM All-Atom Additive Biological Force Fields. *J. Comput. Chem.* **2010**, *31* (4), 671−690.
(64) Jorgensen, W. L.; Chandrasekhar, J.; Madura, J. D.; Impey, R. W.; Klein, M. L. Comparison of Simple Potential Functions for Simulating Liquid Water. *J. Chem. Phys.* **1983**, *79* (2), 926−935.
(65) Laskowski, R. A.; Jabłońska, J.; Pravda, L.; Vařeková, R. S.; Thornton, J. M. PDBsum: Structural Summaries of PDB Entries. *Protein Sci.* **2018**, *27* (1), 129−134.
(66) Yuce, M.; Sarica, Z.; Ates, B.; Kurkcuoglu, O. Exploring Species-Specific Inhibitors with Multiple Target Sites on *S. Aureus* Pyruvate Kinase Using a Computational Workflow. *J. Biomol. Struct. Dyn.* **2023**, *41* (8), 3496−3510.
(67) Liu, X.; Masoudi, A.; Kahsai, A. W.; Huang, L.-Y.; Pani, B.; Staus, D. P.; Shim, P. J.; Hirata, K.; Simhal, R. K.; Schwalb, A. M.; Rambarat, P. K.; Ahn, S.; Lefkowitz, R. J.; Kobilka, B. *Mechanism of b 2 AR Regulation by an Intracellular Positive Allosteric Modulator*. http://science.sciencemag.org/.
(68) Jaeger, K.; Bruenle, S.; Weinert, T.; Guba, W.; Muehle, J.; Miyazaki, T.; Weber, M.; Furrer, A.; Haenggi, N.; Tetaz, T.; Huang, C. Y.; Mattle, D.; Vonach, J. M.; Gast, A.; Kuglstatter, A.; Rudolph, M. G.; Nogly, P.; Benz, J.; Dawson, R. J. P.; Standfuss, J. Structural Basis for Allosteric Ligand Recognition in the Human CC Chemokine Receptor 7. *Cell* **2019**, *178* (5), 1222−1230.e10.
(69) Yang, F.; Mao, C.; Guo, L.; Lin, J.; Ming, Q.; Xiao, P.; Wu, X.; Shen, Q.; Guo, S.; Shen, D.-D.; Lu, R.; Zhang, L.; Huang, S.; Ping, Y.; Zhang, C.; Ma, C.; Zhang, K.; Liang, X.; Shen, Y.; Nan, F.; Yi, F.; Luca, V. C.; Zhou, J.; Jiang, C.; Sun, J.-P.; Xie, X.; Yu, X.; Zhang, Y. Structural Basis of GPBAR Activation and Bile Acid Recognition. *Nature* **2020**, *587* (7834), 499−504.
(70) Zhang, D.; Gao, Z. G.; Zhang, K.; Kiselev, E.; Crane, S.; Wang, J.; Paoletta, S.; Yi, C.; Ma, L.; Zhang, W.; Han, G. W.; Liu, H.; Cherezov, V.; Katritch, V.; Jiang, H.; Stevens, R. C.; Jacobson, K. A.; Zhao, Q.; Wu, B. Two Disparate Ligand-Binding Sites in the Human P2Y1 Receptor. *Nature* **2015**, *520* (7547), 317−321.
(71) Draper-Joyce, C. J.; Bhola, R.; Wang, J.; Bhattarai, A.; Nguyen, A. T. N.; Cowie-Kent, I.; O'Sullivan, K.; Chia, L. Y.; Venugopal, H.; Valant, C.; Thal, D. M.; Wootten, D.; Panel, N.; Carlsson, J.; Christie, M. J.; White, P. J.; Scammells, P.; May, L. T.; Sexton, P. M.; Danev, R.; Miao, Y.; Glukhova, A.; Imlach, W. L.; Christopoulos, A. Positive Allosteric Mechanisms of Adenosine A1 Receptor-Mediated Analgesia. *Nature* **2021**, *597* (7877), 571−576.
(72) Wall, M. J.; Hill, E.; Huckstepp, R.; Barkan, K.; Deganutti, G.; Leuenberger, M.; Preti, B.; Winfield, I.; Carvalho, S.; Suchankova, A.; Wei, H.; Safitri, D.; Huang, X.; Imlach, W.; La Mache, C.; Dean, E.; Hume, C.; Hayward, S.; Oliver, J.; Zhao, F.-Y.; Spanswick, D.; Reynolds, C. A.; Lochner, M.; Ladds, G.; Frenguelli, B. G. Selective Activation of Gαob by an Adenosine A1 Receptor Agonist Elicits Analgesia without Cardiorespiratory Depression. *Nat. Commun.* **2022**, *13* (1), No. 4150.
(73) Glukhova, A.; Thal, D. M.; Nguyen, A. T.; Vecchio, E. A.; Jörg, M.; Scammells, P. J.; May, L. T.; Sexton, P. M.; Christopoulos, A. Structure of the Adenosine A1 Receptor Reveals the Basis for Subtype Selectivity. *Cell* **2017**, *168* (5), 867−877.e13.
(74) Rovati, G. E.; Capra, V.; Neubig, R. R. The Highly Conserved DRY Motif of Class A G Protein-Coupled Receptors: Beyond the Ground State. *Mol. Pharmacol.* **2007**, *71* (4), 959−964.
(75) Abosamak, N. E. R.; Shahin, M. H. *Beta2 Receptor Agonists and Antagonists*. https://www.ncbi.nlm.nih.gov/books/NBK559069/.
(76) Kolmus, K.; Tavernier, J.; Gerlo, S. B2-Adrenergic Receptors in Immunity and Inflammation: Stressing NF-κB. *Brain, Behav., Immun.* **2015**, *45*, 297−310.
(77) Kofuku, Y.; Ueda, T.; Okude, J.; Shiraishi, Y.; Kondo, K.; Maeda, M.; Tsujishita, H.; Shimada, I. Efficacy of the B2-Adrenergic Receptor Is Determined by Conformational Equilibrium in the Transmembrane Region. *Nat. Commun.* **2012**, *3* (1), No. 1045.
(78) Jones, E. M.; Lubock, N. B.; Venkatakrishnan, A.; Wang, J.; Tseng, A. M.; Paggi, J. M.; Latorraca, N. R.; Cancilla, D.; Satyadi, M.; Davis, J. E.; Babu, M. M.; Dror, R. O.; Kosuri, S. Structural and Functional Characterization of G Protein−Coupled Receptors with Deep Mutational Scanning. *eLife* **2020**, *9*, No. e54895.
(79) Stadtmann, A.; Zarbock, A. CXCR2: From Bench to Bedside. *Front. Immun.* **2012**, *3*, No. 263.
(80) Korbecki, J.; Kupnicka, P.; Chlubek, M.; Gorący, J.; Gutowska, I.; Baranowska-Bosiacka, I. CXCR2 Receptor: Regulation of Expression, Signal Transduction, and Involvement in Cancer. *Int. J. Mol. Sci.* **2022**, *23* (4), 2168.
(81) Yang, J.; Richmond, A. Constitutive IkappaB Kinase Activity Correlates with Nuclear Factor-kappaB Activation in Human Melanoma Cells. *Cancer Res.* **2001**, *61* (12), 4901−4909.
(82) Sharma, B.; Nawandar, D. M.; Nannuru, K. C.; Varney, M. L.; Singh, R. K. Targeting CXCR2 Enhances Chemotherapeutic Response, Inhibits Mammary Tumor Growth, Angiogenesis, and Lung Metastasis. *Mol. Cancer Ther.* **2013**, *12* (5), 799−808.
(83) Liu, K.; Wu, L.; Yuan, S.; Wu, M.; Xu, Y.; Sun, Q.; Li, S.; Zhao, S.; Hua, T.; Liu, Z.-J. Structural Basis of CXC Chemokine Receptor 2 Activation and Signalling. *Nature* **2020**, *585* (7823), 135−140.
(84) Missale, C.; Nash, S. R.; Robinson, S. W.; Jaber, M.; Caron, M. G. Dopamine Receptors: From Structure to Function. *Physiol. Rev.* **1998**, *78* (1), 189−225.
(85) Mishra, A.; Singh, S.; Shukla, S. Physiological and Functional Basis of Dopamine Receptors and Their Role in Neurogenesis: Possible Implication for Parkinson's Disease. *J. Exp Neurosci* **2018**, *12*, No. 117906951877982.
(86) Feng, X.-T.; Leng, J.; Xie, Z.; Li, S.-L.; Zhao, W.; Tang, Q.-L. GPR40: A Therapeutic Target for Mediating Insulin Secretion. *Int. J. Mol. Med.* **2012**, *30* (6), 1261−1266.
(87) Moss, R.; Sachse, F. B.; Moreno-Galindo, E. G.; Navarro-Polanco, R. A.; Tristani-Firouzi, M.; Seemann, G. Modeling Effects of Voltage Dependent Properties of the Cardiac Muscarinic Receptor on Human Sinus Node Function. *PLoS Comput. Biol.* **2018**, *14* (10), No. e1006438.
(88) Hirshman, C. A.; Lande, B.; Croxton, T. L. Role of M2Muscarinic Receptors in Airway Smooth Muscle Contraction. *Life Sci.* **1999**, *64* (6−7), 443−448.
(89) Pradhan, A. A.; Befort, K.; Nozaki, C.; Gavériaux-Ruff, C.; Kieffer, B. L. The Delta Opioid Receptor: An Evolving Target for the Treatment of Brain Disorders. *Trends Pharmacol. Sci.* **2011**, *32* (10), 581−590.
(90) Quirion, B.; Bergeron, F.; Blais, V.; Gendron, L. The Delta-Opioid Receptor; a Target for the Treatment of Pain. *Front. Mol. Neurosci.* **2020**, *13*, No. 52.
(91) Granier, S.; Manglik, A.; Kruse, A. C.; Kobilka, T. S.; Thian, F. S.; Weis, W. I.; Kobilka, B. K. Structure of the δ-Opioid Receptor Bound to Naltrindole. *Nature* **2012**, *485* (7398), 400−404.
(92) Wong, T.-S.; Li, G.; Li, S.; Gao, W.; Chen, G.; Gan, S.; Zhang, M.; Li, H.; Wu, S.; Du, Y. G Protein-Coupled Receptors in Neurodegenerative Diseases and Psychiatric Disorders. *Signal Transduction Targeted Ther.* **2023**, *8* (1), No. 177.
(93) Pathan, H.; Williams, J. Basic Opioid Pharmacology: An Update. *Br. J. Pain* **2012**, *6* (1), 11−16.

https://doi.org/10.1021/acsomega.4c06172
ACS Omega 2024, 9, 40154−40171

(94) Wang, Y.; Zhuang, Y.; DiBerto, J. F.; Zhou, X. E.; Schmitz, G. P.; Yuan, Q.; Jain, M. K.; Liu, W.; Melcher, K.; Jiang, Y.; Roth, B. L.; Xu, H. E. Structures of the Entire Human Opioid Receptor Family. *Cell* **2023**, *186* (2), 413−427.e17.
(95) Nordquist, E. B.; Zhao, M.; Kumar, A.; MacKerell, A. D., Jr. Combined Physics- and Machine-Learning-Based Method to Identify Druggable Binding Sites Using SILCS-Hotspots. *J. Chem. Inf. Model.* Accepted for publication, 2024. DOI: 10.26434/chemrxiv-2024-hrqq9-v2.

https://doi.org/10.1021/acsomega.4c06172
ACS Omega 2024, 9, 40154−40171